Title: A descending inhibitory mechanism of nociception mediated by an evolutionarily conserved neuropeptide system in *Drosophila*

Authors: Izumi Oikawa[1], Shu Kondo[2], Kao Hashimoto[3], Akiho Yoshida[1], Megumi Hamajima[4], Hiromu Tanimoto[5], Katsuo Furukubo-Tokunaga[6], Ken Honjo[4, 6*]

Affiliations

[1]Graduate School of Life and Environmental Sciences, University of Tsukuba, Tsukuba, Ibaraki 305-8572, Japan.

[2]Faculty of Advanced Engineering, Tokyo University of Science, Katsushika-ku, Tokyo 125-8585, Japan.

[3]College of Life and Environmental Sciences, University of Tsukuba, Tsukuba, Ibaraki 305-8572, Japan.

[4]Center for Development of Advanced Medicine for Dementia, National Center for Geriatrics and Gerontology, Obu, Aichi 474-8511, Japan.

[5]Graduate School of Life Sciences, Tohoku University, Sendai, Miyagi 980-8577, Japan.

[6]Faculty of Life and Environmental Sciences, University of Tsukuba, Tsukuba, Ibaraki 305-8572, Japan.

*Correspondence: Ken Honjo (khonjo@ncgg.go.jp, khonjo831@gmail.com)

Abstract

Nociception is a neural process that animals have developed to avoid potentially tissue-damaging stimuli. While nociception is triggered in the peripheral nervous system, its modulation by the central nervous system is a critical process in mammals, whose dysfunction has been extensively implicated in chronic pain pathogenesis. The peripheral mechanisms of nociception are largely conserved across the animal kingdom. However, it is unclear whether the brain-mediated modulation is also conserved in non-mammalian species. Here, we show that *Drosophila* has a descending inhibitory mechanism of nociception from the brain, mediated by the neuropeptide Drosulfakinin (DSK), a homolog of cholecystokinin (CCK) that plays an important role in the descending control of nociception in mammals. We found that mutants lacking *dsk* or its receptors are hypersensitive to noxious heat. Through a combination of genetic, behavioral, histological, and Ca^{2+} imaging analyses, we subsequently revealed neurons involved in DSK-mediated nociceptive regulation at a single-cell resolution and identified a DSKergic descending neuronal pathway that inhibits nociception. This study provides the first evidence for a descending modulatory mechanism of nociception from the brain in a non-mammalian species that is mediated by the evolutionarily conserved CCK system, raising the possibility that the descending inhibition is an ancient mechanism to regulate nociception.

Introduction

Minimizing tissue damage is a fundamental task for all animals to increase their chance of survival. Thus, elucidating the principles of nociception, the neural process detecting and encoding potentially tissue-damaging stimuli, is critical to understanding the molecular and neural mechanisms implementing adaptive behaviors and their evolution. Nociceptors are sensory neurons specialized to detect harmful stimuli, whose activation triggers downstream nociceptive circuits and nocifensive responses (1). Since the activities of nociceptors and downstream nociceptive circuits are tightly linked to pain perception in humans, unveiling the mechanisms of nociception is also crucial to a better understanding of human pain mechanisms (2, 3).

Descending inhibition has been suggested to be a pivotal mechanism in the modulation of nociception and pain in mammals. Since the discovery that electrical stimulations of parts of the midbrain in rats enabled surgical operations without anesthetics (4), mammalian descending nociceptive pathways have been implicated in various analgesic phenomena/treatments and the development of chronic pain states, suggesting their critical role in modulating nociception and pain (5, 6). However, brain-mediated modulatory mechanisms of nociception such as descending inhibition have currently been identified only in mammals, despite a high degree of commonality across species in the peripheral nociceptive mechanisms (7, 8). Therefore, it is unknown whether the descending modulation is a *de novo* mechanism typical of the highly developed mammalian central nervous system (CNS) or a conserved control also present in simpler animals.

The descending nociceptive-modulatory systems in mammals have been revealed to involve various

49 neurochemical pathways (5, 6, 9); among these, the cholecystokinin (CCK) system is one of the most extensively
50 characterized (6, 9). In rodents, CCK signaling plays a crucial role in facilitating nociception by counteracting the
51 opioidergic systems in the periaqueductal gray (PAG)—rostral ventral medulla (RVM)—spinal descending pathway
52 (10-13) and inhibiting nociception through the central amygdala (CeA)—PAG—spinal pathway (14). In humans,
53 CCK signaling has been implicated in nocebo hyperalgesia, mediated by the descending nociceptive control system
54 (15). The CCK system is very well-conserved and has been implicated in several common physiological functions
55 among bilaterian species (16-20). However, whether CCK is functionally involved in regulating nociception outside
56 of mammals remains unknown.

57 Drosulfakinin (DSK), a neuropeptide homologous to CCK, was identified in the fruit fly *Drosophila*
58 *melanogaster* (19). Fly DSK is reportedly involved in modulating many physiological functions shared with
59 mammals, including gut functions, anxiety, aggression, memory, feeding, synaptic functions, and courtship
60 behaviors (19, 21-23). After the discovery of stereotyped nociceptive escape behavior called rolling and polymodal
61 Class IV md (C4da) nociceptors (24, 25), the larval *Drosophila* has been successfully utilized to identify
62 evolutionarily conserved and previously uncharacterized molecular pathways in nociception (26-34) and circuitry
63 mechanisms in the ventral nerve cord (VNC; the invertebrate equivalent of the spinal cord) to compute multimodal
64 sensory stimuli and select nociceptive escape strategies (35-40). Previous studies have demonstrated that
65 neuropeptidergic systems also participate in regulating nociception in *Drosophila* (39, 41-44). However, the role of
66 fly DSK in nociception remains elusive.

67 Here, using a collective approach of genetic, behavioral, histological, and Ca^{2+} imaging analyses, we
68 pursued the mechanisms of DSK-mediated nociceptive regulation and demonstrate that the DSK system constitutes
69 a descending inhibitory pathway of nociception from the brain to the VNC in larval *Drosophila.*
70

71 **Results**

72 **DSK signaling negatively regulates thermal nociception**

73 Through a thermal nociception screen using the nocifensive rolling response of *Drosophila* larvae, we found that a
74 deletion mutant line of the *dsk* gene showed thermal hypersensitivity with a significantly shorter latency in their
75 response to a 42 °C probe than the controls, suggesting that DSK plays a role in negatively regulating nociception
76 (Figure 1A and B). A genomic fragment containing the wild-type *dsk* gene, and no other neuropeptide genes,
77 significantly rescued the thermal hypersensitivity of the *dsk* mutants (Figure 1B), confirming that *dsk* is responsible
78 for the thermal hypersensitivity.

79 DSK has been shown to activate two G-protein coupled receptors, CCKLR-17D1 and CCKLR-17D3 (45,
80 46), which are orthologous to the mammalian CCK receptors, CCKAR (also known as CCK_1) and CCKBR (also
81 known as CCK_2) (16-18). To test whether these receptors mediate DSK signaling in nociception, we generated
82 deletion mutants for *CCKLR-17D1* and *CCKLR-17D3* using CRISPR/Cas9 genome editing and tested them for
83 thermal nociception (Figure 1C-F). When stimulated with a 42 °C probe, three independent deletion lines of the
84 *CCKLR-17D1* and *CCKLR-17D3* exhibited thermal hypersensitivity (Figure 1D and F), further supporting the role

85 of DSK signaling in the negative regulation of thermal nociception. To examine whether the phenotypes of *CCKLR-*
86 *17D1* and *CCKLR-17D3* mutants are classified as hyperalgesia (hypersensitivity to normally noxious stimuli) or
87 allodynia (abnormal hypersensitivity to normally innocuous stimuli), we tested the receptor mutants with a 38 °C
88 probe, which is close to the threshold of larval thermal nociception (39 °C) (24). We found that the responses of the
89 DSK receptor mutants were indistinguishable from the controls, indicating that the DSK receptor mutants are
90 hypersensitive to suprathreshold thermal stimuli, thus hyperalgesic (Figure 1-figure supplement 1).

91 We have noticed that the *yw* control strain, which was used by us to generate the *dsk* and receptor deletion
92 mutants, showed relatively longer response latencies to the 42 °C probe compared to the other control strains used
93 in this study. This may be attributed to the effect of the genetic background, although, presently, the cause for this
94 difference is unknown.

95 **Two groups of brain neurons expressing DSK are responsible for regulating nociception**

96 We attempted to identify DSK-expressing cells in the larval CNS that are responsible for regulating nociception.
97 Unlike mammalian CCK, which is expressed in the CNS and gastrointestinal system, *Drosophila* DSK is expressed
98 in the CNS but not in the gut (19, 47-50). Previous immunohistochemical studies have reported putative DSK-
99 expressing cells in the larval CNS (47, 49). However, since the specificity of the DSK antibodies has not been
100 validated with null mutants in the former studies, it has been a concern that the reported DSK-expressing cells could
101 include non-DSK cells that express the other neuropeptides sharing the C-terminal RFa motif with DSK (51).
102 Consistent with this concern, we found that an antibody against crustacean FLRFa, an FMRFa-like neuropeptide

103 with the C-terminal RFa motif, gives rise to a comparable staining pattern to that of the previously reported DSK
104 antibodies, visualizing cells designated as insulin-producing cells (IPCs; referred to as SP3 in Nichols and Lim,
105 (1996) (47)), MP1, SP1, SP2, Sv, SE2, Tv1-3, T2dm, and A8 in the larval CNS (Figure 2A) (47, 49).

106 To identify bona fide DSK-expressing cells responsible for regulating nociception, we performed anti-
107 FLRFa staining in multiple *dsk* null alleles and found that the staining signals persist in all but two pairs of neurons,
108 MP1 and Sv, in the mutant CNS (Figure 2B-D and Figure 2-figure supplement 1A-D), suggesting that these two
109 pairs of neurons are the only neurons in the larval CNS that express DSK. The genomic rescue fragment that rescued
110 the thermal hypersensitivity of *dsk* mutants (Figure 1B) also restored the anti-FLRFa signals in MP1 and Sv in a
111 *dsk* mutant background (Figure 2E), suggesting that the *dsk* gene is responsible for the anti-FLRFa signals in these
112 neurons as well as the thermal nociceptive responses of larvae. This expression pattern was further corroborated by
113 the transgenic reporter line *DSK-GAL4* and the 2A-GAL4 knock-in reporter line *DSK-2A-GAL4* (52), both of which
114 we found were expressed only in MP1 and Sv neurons among the anti-FLRFa-positive neurons (Figure 2A, C, and
115 F; Figure 2-figure supplement 1B-F). We also found that anti-FLRFa, *DSK-GAL4*, and *DSK-2A-GAL4* do not
116 visualize larval peripheral neurons including C4da nociceptors (Figure 2A and F; Figure 2-figure supplement 1G).
117 Taken together, these results identified two sets of brain neurons, MP1 and Sv, as the DSK-expressing cells that are
118 involved in regulating nociception in larvae.

119 **CCKLR-17D1 in Goro neurons functions to negatively regulate nociception**

120 We sought the potential target cells of DSK signaling for regulating nociception. Since DSK receptor mutants were

121 thermally hypersensitive consistently to *dsk* mutants (Figure 1B, D, and F), neurons in the larval nociceptive circuit
122 that express DSK receptors were promising candidates. To visualize the cells expressing DSK receptors, we
123 generated T2A-GAL4 knock-ins in *CCKLR* genes. Both *CCKLR-17D1-T2A-GAL4* and *CCKLR-17D3-T2A-GAL4*
124 were widely expressed in the larval CNS, predominantly in neuronal cells (Figure 3A and B; Figure 3-figure
125 supplement 1A-D). By performing double-labeling experiments, we found that *CCKLR-17D1-T2A-GAL4* and
126 *CCKLR-17D3-T2A-GAL4* are not expressed in the nociceptors at the periphery (Figure 3C and D; Figure 3-figure
127 supplement 1E and F), or in nociceptive interneurons including Basin1-4 (53), A08n (36, 41), and DnB neurons
128 (35) in the larval VNC (Figure 3-figure supplement 1G-L). However, we found that they are expressed in Goro
129 neurons (Figure 3E and F), which are the fourth-order nociceptive interneurons located in the larval VNC (53).
130 To test whether the DSK receptors in Goro neurons are functionally important for regulating nociception,
131 we performed RNAi and rescue experiments using *R69E06-GAL4* that marks Goro neurons (53). RNAi knockdown
132 of CCKLR-17D1, but not CCKLR-17D3, in *R69E06-GAL4* neurons induced thermal hypersensitivity (Figure 4A
133 and Figure 4-figure supplement 1A). *R69E06-GAL4* is also expressed in multiple neurons in the larval brain other
134 than Goro neurons in the VNC (53). However, the thermal hypersensitivity was not observed when the expression
135 of CCKLR-17D1 RNAi was excluded from Goro neurons by *tsh-GAL80*, pointing to the requirement of CCKLR-
136 17D1 in Goro neurons (Figure 4-figure supplement 1B-D). Consistent with these RNAi results, expressing wild-
137 type CCKLR-17D1, but not CCKLR-17D3, with *R69E06-GAL4* rescued the hypersensitivity of the respective
138 mutants (Figure 4B and C). Furthermore, the morphology of Goro neurons was not affected by CCKLR-17D1

139 knockdown (Figure 4-figure supplement 1E). Therefore, we conclude that CCKLR-17D1 functions in Goro neurons
140 to negatively regulate thermal nociception, but the function of CCKLR-17D3 in nociceptive regulations resides
141 elsewhere.

142 Activation of Goro neurons elicits nocifensive rolling in larvae (53). Hence, if CCKLR-17D1 functions
143 in Goro neurons to negatively regulate nociception, the lack of CCKLR-17D1 should sensitize these neurons to
144 noxious heat. We directly addressed this hypothesis by using a Ca^{2+} imaging technique we had previously developed
145 (32, 35), whereby we monitored GCaMP6m signals in Goro neurons while locally applying thermal ramp stimuli
146 to the larval body wall. In our thermal ramp stimulation protocol, the temperature around the larval CNS hardly
147 reached 28 °C during the heat ramp stimulations (27.0 ± 0.2 °C at the peak, n = 12), suggesting that the larval
148 nociceptive system in the CNS that functions as an internal sensor for fast temperature increase (54) was unlikely
149 to be activated.

150 Goro neurons in *CCKLR-17D1*$^{\Delta 1}$ mutants showed a significantly steeper GCaMP6m signal increase from
151 40 to 50 °C in comparison with the wild-type controls (Figure 5A and B, Video 1 and 2). Since the baseline
152 fluorescence levels of GCaMP6m were not significantly different in the wild-type and *CCKLR-17D1*$^{\Delta 1}$ mutants
153 (Figure 5C), these data demonstrate that Goro neurons in *CCKLR-17D1*$^{\Delta 1}$ mutants are specifically sensitized to a
154 noxious range of heat. Suppressing CCKLR-17D1 by RNAi in Goro neurons also induced significantly sensitized
155 responses of Goro to noxious temperatures of 44–49 °C (Figure 5D-F, Video 3 and 4). In contrast, Goro neurons in
156 *CCKLR-17D3*$^{\Delta 1}$ mutants exhibited GCaMP6m signals that were mildly elevated but largely parallel compared with

157 that of the controls (Figure 5-figure supplement 1, Video 5 and 6), providing further evidence for the major
158 functioning of CCKLR-17D3 in nociceptive regulation outside Goro neurons. Considered together, these data
159 demonstrate that CCKLR-17D1 functions to negatively regulate the activity of Goro neurons, thereby attenuating
160 behavioral nociceptive responses.

161 **Neuronal projections and thermal responsiveness of DSK-expressing neurons**

162 If CCKLR-17D1 is involved in regulating the activity of Goro neurons, how can DSK be conveyed from the brain
163 to the VNC? We noticed that some of the *DSK-GAL4* positive brain neurons sent descending neural processes to
164 the VNC (Figure 6A), which were all anti-FLRFa positive (Figure 6B). Furthermore, the anti-FLRFa signals in the
165 descending projections were completely absent in the *dsk* mutants (Figure 6C), suggesting that these descending
166 projections likely originated from the DSK-expressing brain cells, namely MP1 and/or Sv. In analyzing *DSK-2A-*
167 *GAL4*, we found that MP1 neurons in fact sent the descending projections to the VNC (Figure 6D). To further
168 understand the projection patterns of MP1 and Sv neurons in detail, we performed single-cell labeling using an
169 FLP-out technique and revealed that MP1 neurons sent descending projections contralaterally to the VNC (Figure
170 6E), while Sv neurons projected within the brain (Figure 6F). In comparison with the longitudinal processes to the
171 VNC, MP1 neural processes in the brain possessed few anti-FLRFa positive puncta, which represent DSK in these
172 neurons (Figure 6G). Furthermore, when the somatodendritic marker *UAS-Denmark* (55) and the synaptic vesicle
173 marker *UAS-syt::eGFP* were expressed in MP1 neurons, Denmark preferentially localized in the neural processes
174 within the brain while syt::eGFP strongly accumulated in the processes descending to the VNC (Figure 6H).

175 Collectively, these data demonstrate that MP1 neurons project DSK-positive descending axons to the VNC from
176 the brain.

177 Next, we investigated whether some of these DSK-expressing neurons are responsive to noxious thermal
178 stimuli. In order to examine the responsiveness of multiple neurons in intact larvae, we took the snapshot approach
179 using CaMPARI, a genetically-encoded Ca^{2+} sensor whose fluorescence irreversibly changes from the green to the
180 red region of the spectrum in response to irradiation with 405 nm UV light in a Ca^{2+} dependent manner, and is thus
181 useful to monitor the activities of multiple neurons simultaneously in intact animals (56). When the larvae
182 expressing CaMPARI2 (an improved version of CaMPARI (57)) in Goro neurons were stimulated by local thermal
183 ramp stimuli under a 405 nm UV light, a significantly increased CaMPARI2 photoconversion was detected
184 compared to the control group that had only been irradiated with 405nm UV (Figure 7A and B), confirming that by
185 using CaMPARI2 in our experimental setup we managed to successfully capture the increased activity of Goro
186 neurons in response to noxious heat in intact larvae. We then tested the responsiveness of *DSK-2A-GAL4* neurons
187 using the same stimulation and photoconversion protocol and found that none of the MP1 or Sv neurons, nor IPCs
188 showed increased CaMPARI2 photoconversion in response to local thermal ramp stimuli (Figure 7A, C-E).
189 Interestingly, MP1 neurons exhibited high CaMPARI2 photoconversion regardless of the presence of local heat
190 ramp stimuli, which was even comparable to that observed in Goro neurons activated by noxious heat stimuli
191 (Figure 7A and C). These data suggest that none of the *DSK-2A-GAL4* neurons are clearly responsive to noxious
192 heat, but the markedly high CaMPARI2 photoconversion observed in MP1 neurons raises the possibility that these

193 neurons may be active regardless of the presence of noxious heat stimuli.

194 **Connectivity between DSKergic and Goro neurons**

195 To gain more insights into the connectivity between DSK-expressing brain neurons and Goro neurons, we
196 further examined the anatomical relationship between MP1 axons and Goro neurons in the VNC. Performing
197 double-labeling experiments, we found that MP1 axons with anti-FLRFa signals (representing DSK in MP1 axons)
198 partially overlapped with Goro neurites in the thoracic segments of the larval VNC (Figure 8A). GFP reconstitution
199 was reproducibly detected between MP1 and Goro neurons using the CD4-GRASP (GFP Reconstitution Across
200 Synaptic Partners) system (58, 59), thus confirming that MP1 axons and Goro neurons are indeed in close proximity
201 (Figure 8B). Since the CD4-GRASP is known to detect general cell-cell contacts (60, 61), we further investigated
202 whether MP1 and Goro neurons are synaptically connected by using the nSyb-GRASP technique, which specifically
203 enables synapse detection by localizing one of the split-GFP fragments in presynaptic sites (62). However, no
204 signals of reconstituted GFP were detected between MP1 and Goro with nSyb-GRASP, although we found
205 proximate localizations of nSyb-GFP_{1-10} in the MP1 axons with the Goro neurites expressing CD4::GFP_{11} (Figure
206 8C). We also employed the *trans*-Tango system (63) as another tool to detect synaptic connectivity. However, when
207 the *trans*-Tango ligand was expressed by *DSK-2A-GAL4,* synaptic connectivity between MP1 and Goro was not
208 indicated since the postsynaptic activation of *trans*-Tango signals was not observed in Goro neurons, although some
209 *trans*-Tango-positive neurons were observed around Goro neurons (Figure 8D).

210 Although we could not find positive evidence for synaptic connectivity between MP1 axons and Goro

211 neurons, we further tested the hypothesis that DSK-expressing neurons in the brain may have functional
212 connectivity to Goro neurons. To achieve this, we first attempted artificial activation experiments of *DSK-2A-GAL4*
213 neurons using *UAS-dTRPA1* to determine whether activating DSK-expressing neurons actually attenuates larval
214 nociception. dTRPA1 is a cation channel gated by warm temperature (> 29 °C) that has been used as a tool to
215 artificially activate neurons of interest in *Drosophila* (64). When the larvae expressing dTRPA1 in C4da nociceptors
216 with *ppk1.9-GAL4* were placed in a chamber at 35°C, dTRPA1-induced thermogenetic activation of C4da
217 nociceptors caused nocifensive rolling responses within two seconds in the majority of animals, as reported
218 previously (65) (Figure 9A and B). In contrast, when the larvae expressing dTRPA1 simultaneously in *ppk1.9-GAL4*
219 and *DSK-2A-GAL4* were placed in a chamber at 35°C, the additional activation of *DSK-2A-GAL4* neurons to C4da
220 nociceptors resulted in a markedly reduced percentage of larvae showing rolling responses within two seconds and
221 in significantly lengthened latencies to exhibit a rolling response (Figure 9A and B). None of the animals expressing
222 dTRPA1 with *DSK-2A-GAL4* alone showed a rolling response within 10 seconds (Figure 9A).

223 The above data suggest that activation of *DSK-2A-GAL4* neurons inhibits larval nociception. We then
224 investigated whether activating *DSK-2A-GAL4* neurons could attenuate the activity of Goro neurons, by combining
225 the artificial activation experiments described above with CaMPARI2 snapshot imaging of Goro neurons. Indeed,
226 CaMPARI2 photoconversion in Goro neurons induced by the thermogenetic activations of C4da nociceptors was
227 significantly decreased by 35% with the simultaneous activation of *DSK-2A-GAL4* neurons (Figure 9C and D).
228 Given that MP1 neurons were the only cells that were labeled by *DSK-2A-GAL4* with 100% reproducibility, while

229 the expression of *DSK-2A-GAL4* in IPCs and Sv neurons was minor and stochastic (Figure 2F), the observed
230 inhibition of behavioral nociception and Goro neurons caused by activating *DSK-2A-GAL4* neurons is mostly
231 attributable to the activation of MP1 neurons. Thus, these data support the functional connectivity between
232 DSKergic MP1 neurons in the brain and Goro neurons.
233

234 **Discussion**

235 In this study, we have demonstrated that (1) DSK and its receptors CCKLR-17D1 and CCKLR-17D3 are involved
236 in negatively regulating thermal nociception, (2) Two sets of brain neurons, MP1 and Sv, express DSK in the larval
237 nervous system, (3) One of the DSK receptors (CCKLR-17D1) functions in Goro neurons in the VNC to negatively
238 regulate thermal nociception, and (4) Thermogenetic activation of *DSK-2A-GAL4* neurons attenuates both larval
239 nociception and the activity of Goro neurons. Based on these results, we propose that the DSKergic neurons
240 regulating the activity of Goro neurons constitute a descending inhibitory pathway of nociception from the brain to
241 the VNC in larval *Drosophila* (Figure 10). To our knowledge, our findings represent the first evidence of a
242 descending mechanism modulating nociception from the brain in a non-mammalian species.

243 **DSKergic descending system as a physiological modulator of nociception**

244 DSK has been implicated in multiple physiological and developmental processes in *Drosophila* (19, 21-23).
245 Previous studies have shown that *dsk* and *CCKLR-17D1* mutants exhibit significant reductions of synaptic growth
246 and excitability in larval neuromuscular junctions (NMJ) and larval locomotion under bright light (45, 66),

247 suggesting the importance of the DSK/CCKLR-17D1 signaling pathway in the developmental processes of
248 motoneurons. However, in this study, no major developmental defects were observed in Goro neurons with CCKLR-
249 17D1 RNAi (Figure 4-figure supplement 1E). Furthermore, the simultaneous thermogenetic activations of *DSK-*
250 *2A-GAL4* neurons and C4da nociceptors inhibited larval nociception and the activity of Goro neurons (Figure 9).
251 Given the pronociceptive role of Goro neurons, their reduced synaptic or neuronal activity should cause nociceptive
252 insensitivity or reduced Ca^{2+} responses, which is contradicting to our observation that CCKLR-17D1 knockdown
253 in Goro produced the thermal hypersensitivity and exaggerated Ca^{2+} responses (Figure 4 and 5). Thus, these data
254 consistently support a physiological role for DSKergic descending signals in the modulation of the activity of Goro
255 neurons rather than a developmental role, highlighting the functional differences of the DSK/CCKLR-17D1
256 pathway between the NMJ and the nociceptive system in the CNS.

257 **DSK in larval IPCs dispensable for nociceptive modulation**

258 A previous study has reported the expression of DSK in a population of larval IPCs and its functions in responding
259 to starving conditions (49). However, we observed that anti-FLRFa signals in IPCs persisted in *dsk* null mutants
260 and that anti-FLRFa signals in IPCs hardly overlap with either *DSK-GAL4* or *DSK-2A-GAL4* expressions (Figure 2
261 and Figure 2-figure supplement 1). Although we used a different antibody from that in the study mentioned above,
262 the number of IPCs visualized by anti-FLRFa was comparable to that of cells visualized by anti-DSK (Figure 2-
263 figure supplement 1) (49). Regarding the functions of IPCs in nociception, Im et al. showed that silencing *dilp2-*
264 *GAL4* positive IPCs has no significant effect on the baseline nociceptive responses (67). In our CaMPARI2 imaging,

265 IPCs marked by *DSK-2A-GAL4* showed very low baseline activity and no responsiveness to noxious heat (Figure
266 7). Thus, the current and previous studies strongly suggest that IPCs are likely irrelevant for DSK-mediated
267 nociceptive regulation, at least under normal conditions, although it is still possible for DSK to be expressed
268 stochastically in a limited population of IPCs.

269 **Functional mechanisms of DSKergic nociceptive inhibitory system**

270 Although our data suggest the existence of a DSKergic descending inhibitory system from the brain to the Goro
271 neurons in the VNC, there are multiple remaining questions for future studies on the mechanisms by which DSK-
272 expressing neurons in the brain regulate Goro neurons: First, whether both MP1 and Sv neurons are involved in
273 nociceptive inhibition remains unclear. Our findings consistently point to MP1 neurons over Sv neurons as a major
274 source of DSK regulating Goro neurons. However, given the potential of DSK for distant actions through diffusion,
275 the possibility of Sv neurons communicating with Goro neurons cannot be eliminated. Further analysis using finer
276 genetic/neuronal tools will be necessary to tease the functions of MP1 and Sv neurons apart and understand the
277 functional mechanism of the DSKergic system in the regulation of larval nociception.

278 Second, how this DSKergic system is activated to regulate nociception *in vivo* needs further investigation.
279 We observed very high CaMPARI2 photoconversion in MP1 neurons without noxious heat stimuli, which did not
280 further increase in response to noxious heat application (Figure 7). These data raise the hypothesis that MP1 neurons
281 may function as a tonically active brake for nociceptive circuits, rather than a simple negative feedback system that
282 is activated by nociceptive stimuli as input. The tonically active model of MP1 function is also consistent with our

283 data showing that *dsk* and *CCLR-17D1* mutations, as well as CCLR-17D1 RNAi in Goro neurons, all caused thermal
284 hypersensitivity under normal conditions (Figure 1 and 4). Up to this point, no external or internal signals have been
285 directly shown to be the input into larval DSKergic neurons. However, since DSK has been implicated in the
286 regulation of several physiological processes such as hunger and stress, sensory or molecular signals that are
287 involved in these physiological processes have the potential to serve as upstream cues that activate DSKergic
288 neurons. Alternatively, it is also possible that MP1 neurons may have spontaneous activity. Further physiological
289 studies on the activity and responsiveness of DSKergic neurons would be required to elucidate how the DSKergic
290 system functions to regulate nociception in larvae under normal conditions.

291 Third, the transmission mechanisms of DSK from the brain to Goro neurons need further clarification.
292 Our nSyb-GRASP and *trans*-Tango experiments consistently showed negative results, indicating no synaptic
293 connectivity between MP1 descending axons and Goro neurons (Figure 8). Thus, the interaction between DSK from
294 DSKergic neurons in the brain and Goro neurons in the VNC may be mediated non-synaptically through volume
295 transmission, as described in many neuropeptidergic systems (68). Many of the CCKLR-expressing neurons in the
296 VNC are distantly located from the descending MP1 axons (Figure 3 and 6). Since it is unlikely that all these
297 CCKLR-expressing neurons are synaptically connected to MP1 axons, neuronal communications through volume
298 transmission can be fairly assumed for DSKergic systems in the larval VNC. More detailed analyses at an electron
299 microscopic level of the circuitry connectivity between MP1 and Goro neurons and of the localization of DSK-
300 containing vesicles in DSKergic neurons as well as DSK receptors in Goro neurons would be necessary to further

301 clarify the transmission mechanisms of DSK from the brain to Goro neurons.

302 **Multiple molecular pathways for DSK signaling in the regulation of nociception**

303 The data presented in this study also suggest that DSK signaling could regulate larval nociception through multiple
304 pathways other than the DSK/CCKLR-17D1 system. For example, while *CCKLR-17D3* mutants exhibited as severe
305 thermal hypersensitivity as *CCKLR-17D1* mutants (Figure 1D and F), our RNAi and rescue experiments failed to
306 locate the function of CCKLR-17D3 to Goro neurons (Figure 4A and C). Our GCaMP Ca^{2+} imaging also revealed
307 that Goro neurons lacking CCKLR-17D3 showed modestly sensitized responses to noxious heat (Figure 5-figure
308 supplement 1). These results suggest the major functioning of CCKLR-17D3 in Goro-independent nociceptive
309 pathways. We also observed that DSK receptor mutants exhibited more severe thermal phenotypes than *dsk* mutants
310 (Figure 1), which may indicate the presence of unidentified DSK- or CCKLR-dependent signaling pathways in
311 nociception-related cells. Further research is apparently necessary to reveal the whole picture of nociceptive
312 regulations mediated by DSK and its receptors in larval *Drosophila*.

313 **Potential conservation of CCK-mediated descending nociceptive controls**

314 The CCK system is thought to be one of the most ancient neuropeptide systems, suggested to have multiple
315 common physiological functions across taxa (16-20). In this study, we demonstrate that CCKergic signaling in
316 *Drosophila* participates in nociceptive modulation through a descending inhibitory pathway similarly to the
317 mammalian CCK system, adding new evidence about the conserved physiological roles of CCK.

318 Unlike the peripheral nociceptive systems, it is still challenging to align the *Drosophila* and mammalian

319 CCKergic descending pathways due to low homologies of the CNS structures between *Drosophila* and mammals,
320 wide-spread CCK expression in the mammalian CNS, and the multiple roles of the CCKergic systems in
321 mammalian nociceptive controls (10-14, 69-73). However, the common usage of an orthologous molecular pathway
322 in descending controls of nociception between the two evolutionarily distant clades raises a fascinating new
323 hypothesis that the descending control from the brain may also be an ancient, conserved mechanism of nociception,
324 which has emerged in the common ancestor of protostomes and deuterostomes. It will be of interest for future
325 research to investigate whether the role of CCK signaling in descending nociceptive controls is also present in other
326 species.

327 **Potentials of non-mammalian models to study the mechanisms of pain modulation and pain pathology in the**
328 **CNS**

329 Non-mammalian model systems have been increasingly recognized as powerful tools to identify novel pain-related
330 molecular pathways (2, 74-77). However, the utilization of these models has so far been mostly limited to the
331 research on peripheral pain pathophysiology, and few studies have used them to investigate central pain
332 pathophysiology (2, 78). Descending nociceptive control mechanisms are crucial for central pain modulation and
333 have been implicated in the development of chronic pain states in humans (5, 6). Thus, the current study opens the
334 door to a new approach to using powerful neurogenetic tools and the simpler nervous system of *Drosophila* for
335 elucidating the functional principles of descending nociceptive systems, which may potentially contribute to our

336 understanding of the mechanisms underlying central pain modulation and pain pathology due to dysfunctions of
337 descending modulatory pathways.
338

339 **Acknowledgments**

340 We thank the NIG-Fly Stock Center, TRiP at Harvard Medical School (NIH/NIGMS R01-GM084947), the
341 Bloomington Stock Center, and Drs. Masayuki Koganezawa, Takeshi Awasaki, Barry Ganetzky, and Marta Zlatic
342 for fly stocks. We are grateful to Dr. Eve Marder for kindly providing the anti-FLRFa antibody. We also thank Drs.
343 Yoshiki Hayashi, Makoto Hayashi, and Satoru Kobayashi for their support in imaging with Leica SP5 and SP8.
344 This study was supported by grants from JSPS KAKENHI to K Honjo (17K14928, 19K06935, and 22K06328) and
345 HT (17H01378 and 26250001), and grants from the National Center for Geriatrics and Gerontology (21-47), the
346 Uehara Memorial Foundation, and the Mochida Memorial Foundation for Medical and Pharmaceutical Research to
347 K Honjo.
348

349 **Author contributions:** K Honjo conceived the research. IO, K Hashimoto, AY, MH, and K Honjo performed
350 experiments and analyzed data. SK and HT generated dsksk1 mutant and DSK receptor GAL4 lines. K Honjo wrote
351 the manuscript with input and edits from IO, SK, HT, and KFT.
352

353 **Declaration of interests:** Authors declare no competing interests.

354 **Figures**

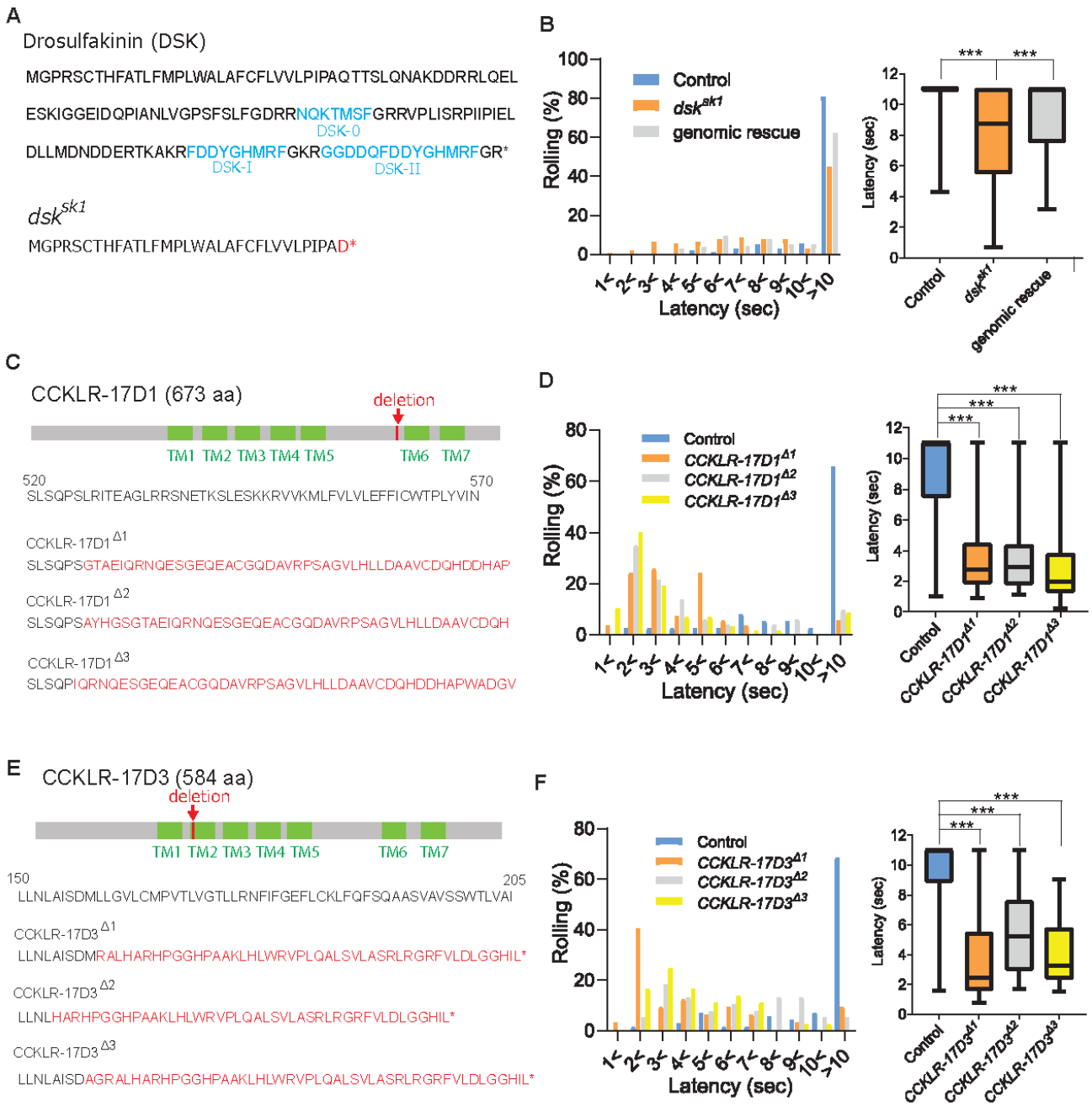

355

356 **Figure 1. DSK signaling is involved in negatively regulating nociception.**

357 (A) Predicted amino acid sequences of pro-DSK peptide in the wild-type (top) and *dsk*^{sk1} mutants (bottom). Due to

358 a 5-base deletion at the +94-99 position in the coding sequence, *dsk*^{sk1} mutants are predicted to produce a largely
359 truncated pro-DSK peptide unable to be processed to active DSK peptides. Red letters represent residues different
360 from the wild-type and asterisks indicate stop codons. (B) Hypersensitivity of *dsk*^{sk1} mutants to a 42°C thermal
361 probe. Significantly shortened latencies of *dsk*^{sk1} mutants (n = 143) compared with the controls (n = 164) were
362 recovered in genomic rescue animals (*Dp(3;1)2-2*; *dsk*^{sk1}, n = 139). (Left) Histograms (Right) Box plots of latencies.
363 *** $p < 0.001$ Steel's test. (C) Predicted amino acid sequence of CCKLR-17D1 in the wild-type and *CCKLR-17D1*
364 mutants. *CCKLR-17D1*$^{\Delta 1}$, *CCKLR-17D1*$^{\Delta 2}$, and *CCKLR-17D1*$^{\Delta 3}$ have 17-base (+1573-1589), 2-base (+1575-1576)
365 and 32-base (+1573-1604) deletions in the coding sequence respectively, which result in large frameshifts
366 completely abolishing the sixth and seventh transmembrane domains (TMs). (D) *CCKLR-17D1*$^{\Delta 1}$ (n = 54), *CCKLR-*
367 *17D1*$^{\Delta 2}$ (n = 51) and *CCKLR-17D1*$^{\Delta 3}$ mutants (n = 57) all showed significantly shorter latencies than control (n =
368 38). (Left) Histograms (Right) Box plots of latencies. *** $p < 0.001$ Steel's test. (E) Predicted amino acid sequence
369 of CCKLR-17D3 in the wild-type and *CCKLR-17D3* mutants. *CCKLR-17D3*$^{\Delta 1}$, *CCKLR-17D3*$^{\Delta 2}$, and *CCKLR-*
370 *17D3*$^{\Delta 3}$ possess 8-base (+474-481), 32-base (+457-488), and 5-base (+472-476) deletions in the coding sequence
371 respectively, which result in large frameshifts and truncation in the middle of the second TM. (F) *CCKLR-17D3*$^{\Delta 1}$
372 (n = 32), *CCKLR-17D3*$^{\Delta 2}$ (n = 38), and *CCKLR-17D3*$^{\Delta 3}$ mutants (n = 36) all exhibited significantly shorter latencies
373 than control (n = 70). (Left) Histograms (Right) Box plots of latencies. *** $p < 0.001$ Steel's test. All box plots
374 show median (middle line) and 25th to 75th percentiles with whiskers indicating the smallest to the largest data
375 points.

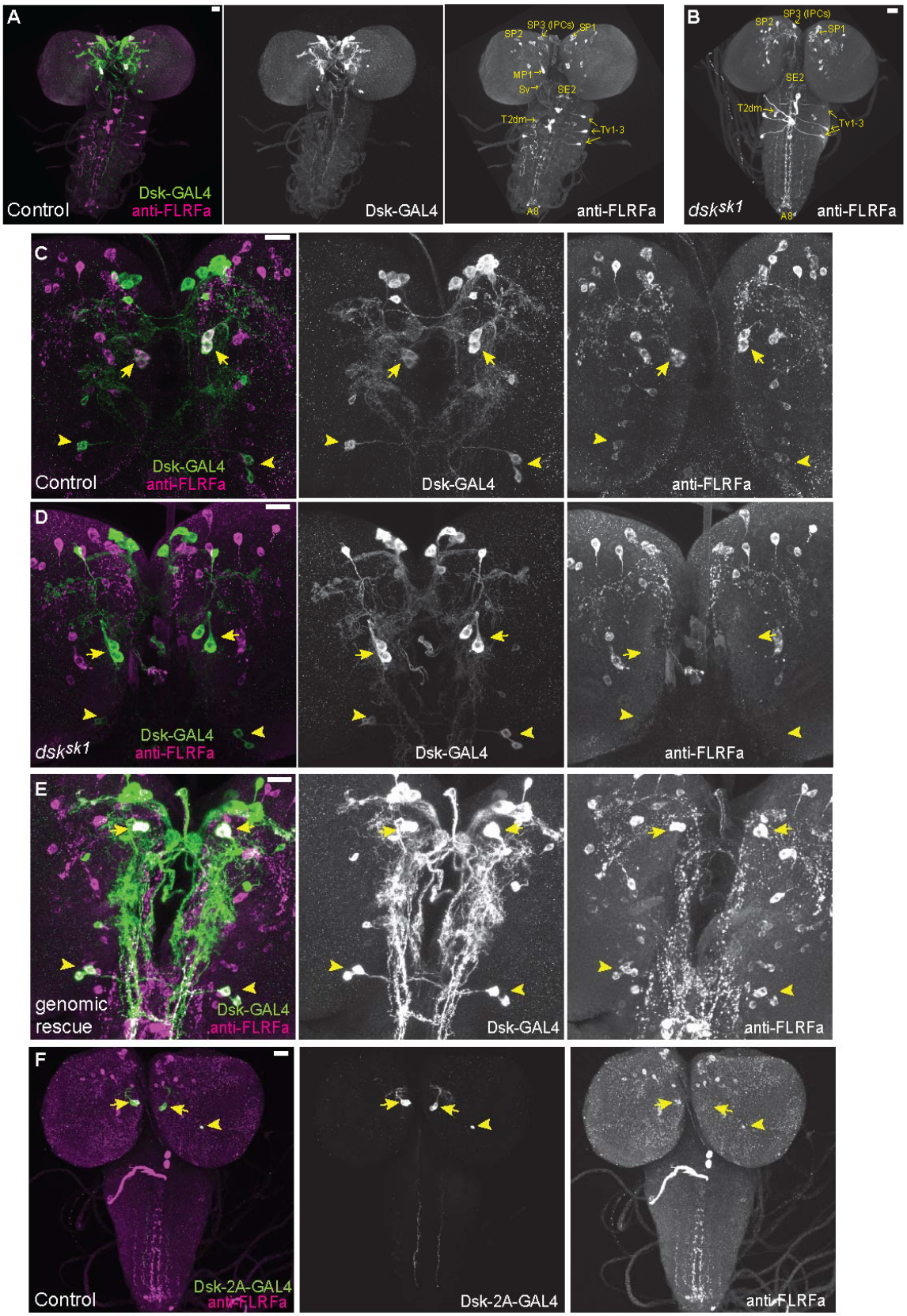
A
Control
Dsk-GAL4
anti-FLRFa
Dsk-GAL4
SP3 (IPCs)
SP1
SP2
MP1
Sv
SE2
T2dm
Tv1-3
A8
anti-FLRFa
B
SP3 (IPCs)
SP2
SP1
SE2
T2dm
Tv1-3
A8
dsksk1
anti-FLRFa
C
Control
Dsk-GAL4
anti-FLRFa
Dsk-GAL4
anti-FLRFa
D
dsksk1
Dsk-GAL4
anti-FLRFa
Dsk-GAL4
anti-FLRFa
E
genomic
rescue
Dsk-GAL4
anti-FLRFa
Dsk-GAL4
anti-FLRFa
F
Control
Dsk-2A-GAL4
anti-FLRFa
Dsk-2A-GAL4
anti-FLRFa

376

377 **Figure 2. DSK is expressed in two groups of larval brain neurons.**

378 (A) Representative image of *DSK-GAL4* expression and anti-FLRFa staining in the wild-type larval CNS. (B)
379 Representative image of anti-FLRFa staining in dsk^{sk1} larval CNS. (C) Representative images of *DSK-GAL4*
380 expression and anti-FLRFa staining in the control larval brains. Arrows and arrowheads indicate MP1 and Sv
381 neurons, respectively. Co-expressions of DSK-GAL4 and anti-FLRFa were observed in MP1 and Sv in all of the
382 examined samples (n = 27/27), but in IPCs only in 7% (n = 2/27). (D) Representative images of *DSK-GAL4*
383 expression and anti-FLRFa staining in the dsk^{sk1} larval brains. Arrows and arrowheads indicate MP1 and Sv neurons,
384 respectively. (E) Representative images of *DSK-GAL4* expression and anti-FLRFa staining in the larval brains of
385 the genomic rescue genotype (*Dp(3;1)2-2*/Y; +/*lexA-rCD2::RFP UAS-mCD8::GFP*; dsk^{sk1} *DSK-GAL4*/dsk^{sk1}).
386 Arrows and arrowheads indicate MP1 and Sv neurons, respectively. (F) An example image showing the expression
387 of *DSK-2A-GAL4*, a 2A-GAL4 knock-in line of the *dsk* gene, more faithfully recapitulating its endogenous
388 expression. Arrows and arrowheads indicate MP1 and Sv neurons, respectively. MP1 neurons were labeled in 100%
389 of *DSK-2AGAL4* samples (n = 41/41), while a single IPC in 51.2% (n = 21/41), multiple IPCs in 24.4% (n = 10/41),
390 and Sv neurons in 17.1% (n = 7/41) of examined samples. All scale bars represent 20 μm.

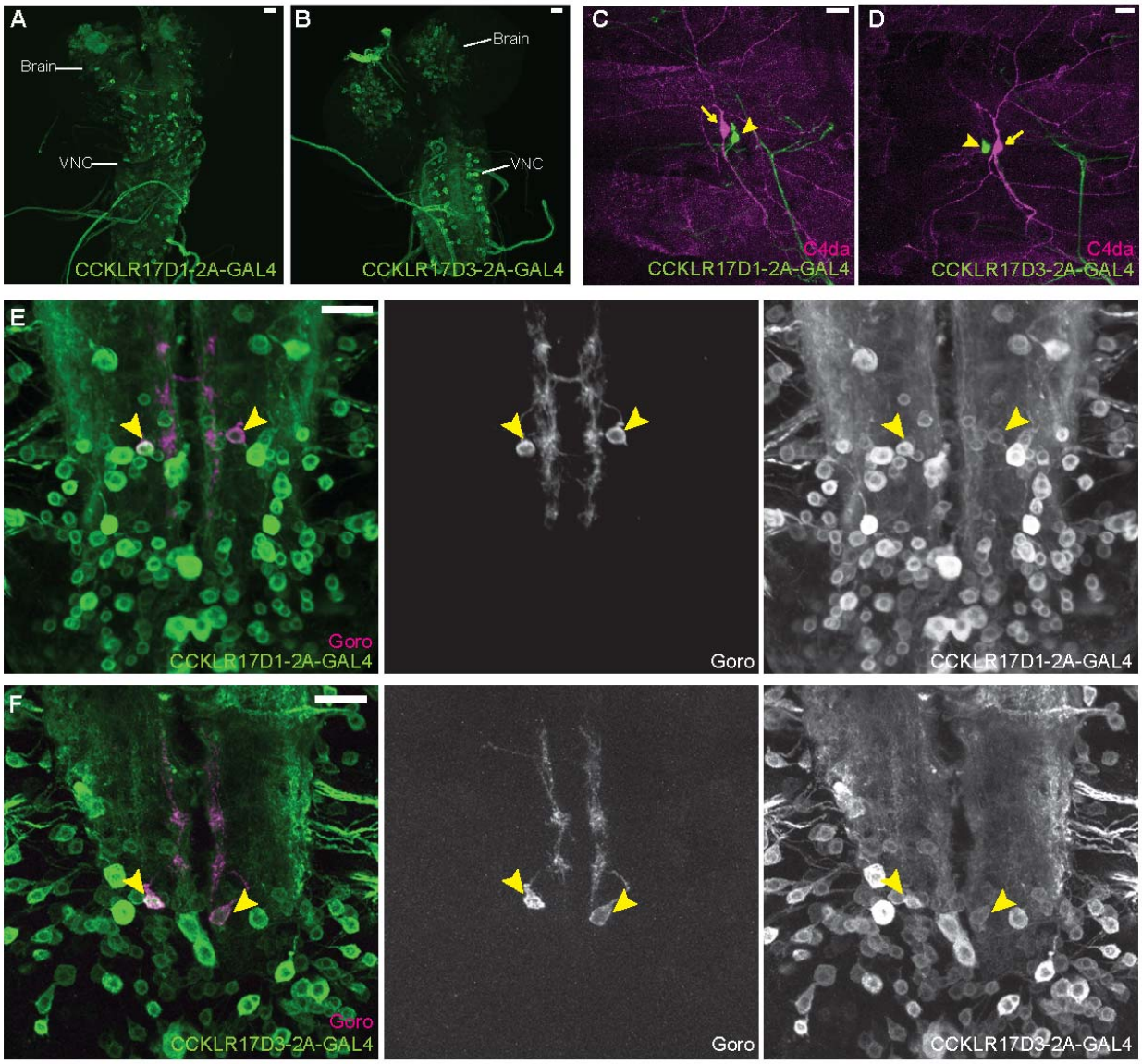

Figure 3. DSK receptors are expressed in Goro neurons in the larval VNC.

(A and B) Representative images of *CCKLR-17D1-T2A-GAL4* (A) and *CCKLR-17D3-T2A-GAL4* (B) expressions in the larval CNS. (C and D) Representative images showing double-labeling of *CCKLR-17D1-T2A-GAL4* (C) and *CCKLR-17D3-T2A-GAL4* (D) with C4da nociceptors (*R38A10-lexA*). Arrows and arrowheads indicate cell bodies of C4da nociceptors and es cells, respectively. (E and F) Representative images showing double-labeling of *CCKLR-*

397 *17D1-T2A-GAL4* (E) and *CCKLR-17D3-T2A-GAL4* (F) with Goro neurons (arrowheads, *R69E06-lexA*). Expression

398 patterns were confirmed in multiple samples (n = 7 and 5). All scale bars represent 20 µm.

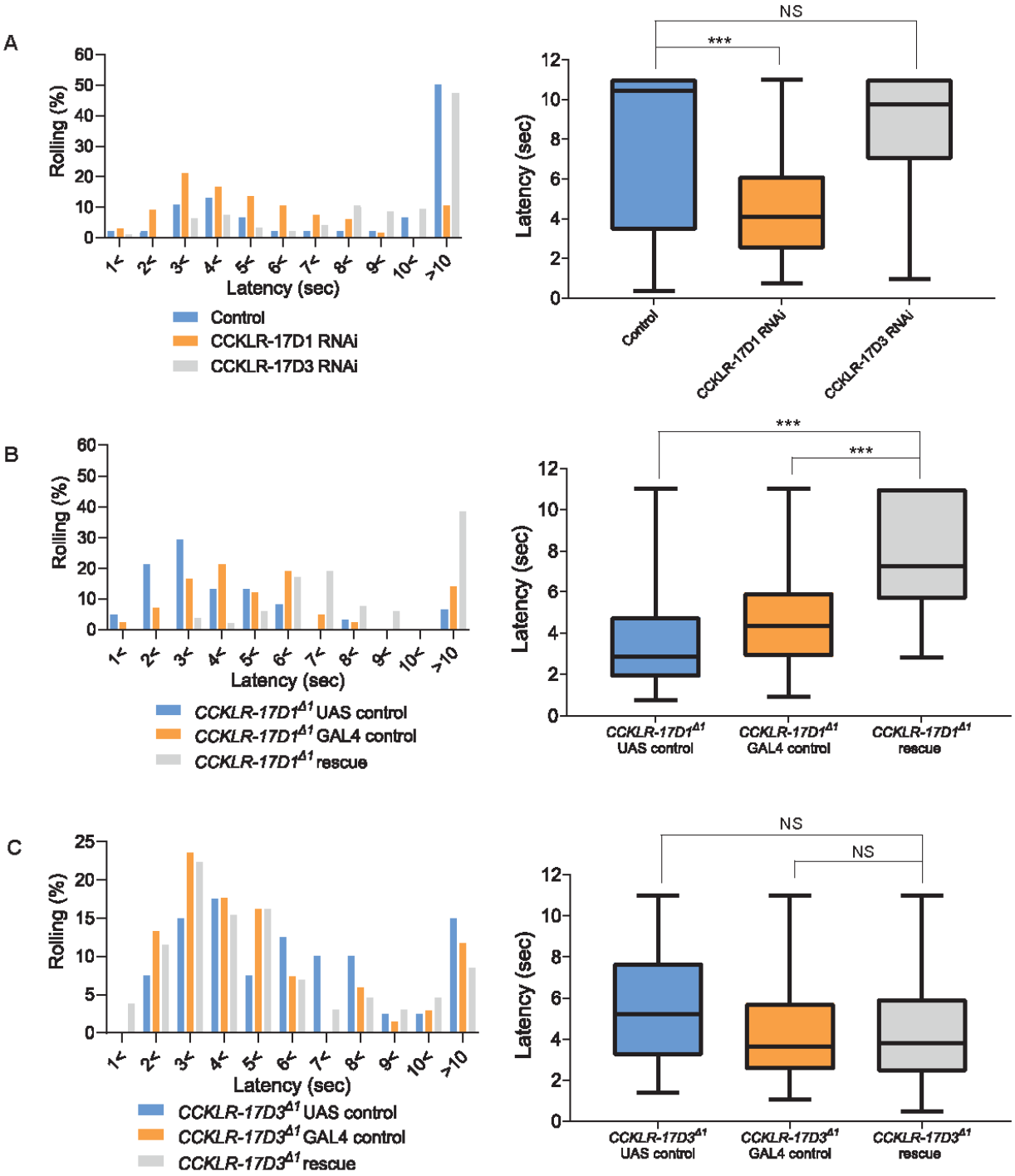

Figure 4. CCKLR-17D1 in Goro neurons is necessary and sufficient for normal thermal nociception.

401 (A) RNAi of CCKLR-17D1 and CCKLR-17D3 using a Goro-GAL4 line *R69E06-GAL4*. Expressing CCKLR-17D1

402 RNAi (*R69E06-GAL4* x *yv; JF02644,* n = 66) but not CCKLR-17D3 RNAi (*R69E06-GAL4* x *yv; JF02968,* n = 95)

403 with *R69E06-GAL4* caused significantly shorter latencies to 42 °C than controls (*R69E06-GAL4* x *yv; attp2,* n =

404 46). (Left) Histograms (Right) Box plots of latencies. *** $p < 0.001$, NS (non-significant) $p > 0.05$ Steel's test. (B)

405 Rescue of CCKLR-17D1 with *R69E06-GAL4*. The shortened latencies of *CCKLR-17D1*$^{\Delta 1}$ mutants observed in UAS

406 controls (*CCKLR-17D1*$^{\Delta 1}$; *UAS-CCKLR-17D1/+,* n = 61) or GAL4 controls (*CCKLR-17D1*$^{\Delta 1}$; *R69E06-GAL4/+,* n

407 = 42) were restored in the rescue genotype (*CCKLR-17D1*$^{\Delta 1}$; *UAS-CCKLR-17D1/+; R69E06-GAL4/+,* n = 52).

408 (Left) Histograms (Right) Box plots of latencies. *** $p < 0.001$ Steel's test. (C) Rescue of CCKLR-17D3 with

409 *R69E06-GAL4*. The shortened latencies of *CCKLR-17D3*$^{\Delta 1}$ mutants were unaltered in the rescue genotype (*CCKLR-*

410 *17D3*$^{\Delta 1}$; *UAS-CCKLR-17D3/+; R69E06-GAL4/+,* n = 130) compared with UAS controls (*CCKLR-17D3*$^{\Delta 1}$; *UAS-*

411 *CCKLR-17D3/+,* n = 40) or GAL4 controls (*CCKLR-17D3*$^{\Delta 1}$; *R69E06-GAL4/+,* n = 68). (Left) Histograms (Right)

412 Box plots of latencies. NS (non-significant) $p > 0.05$ Steel's test. All box plots show median (middle line) and 25th

413 to 75th percentiles with whiskers indicating the smallest to the largest data points.

414

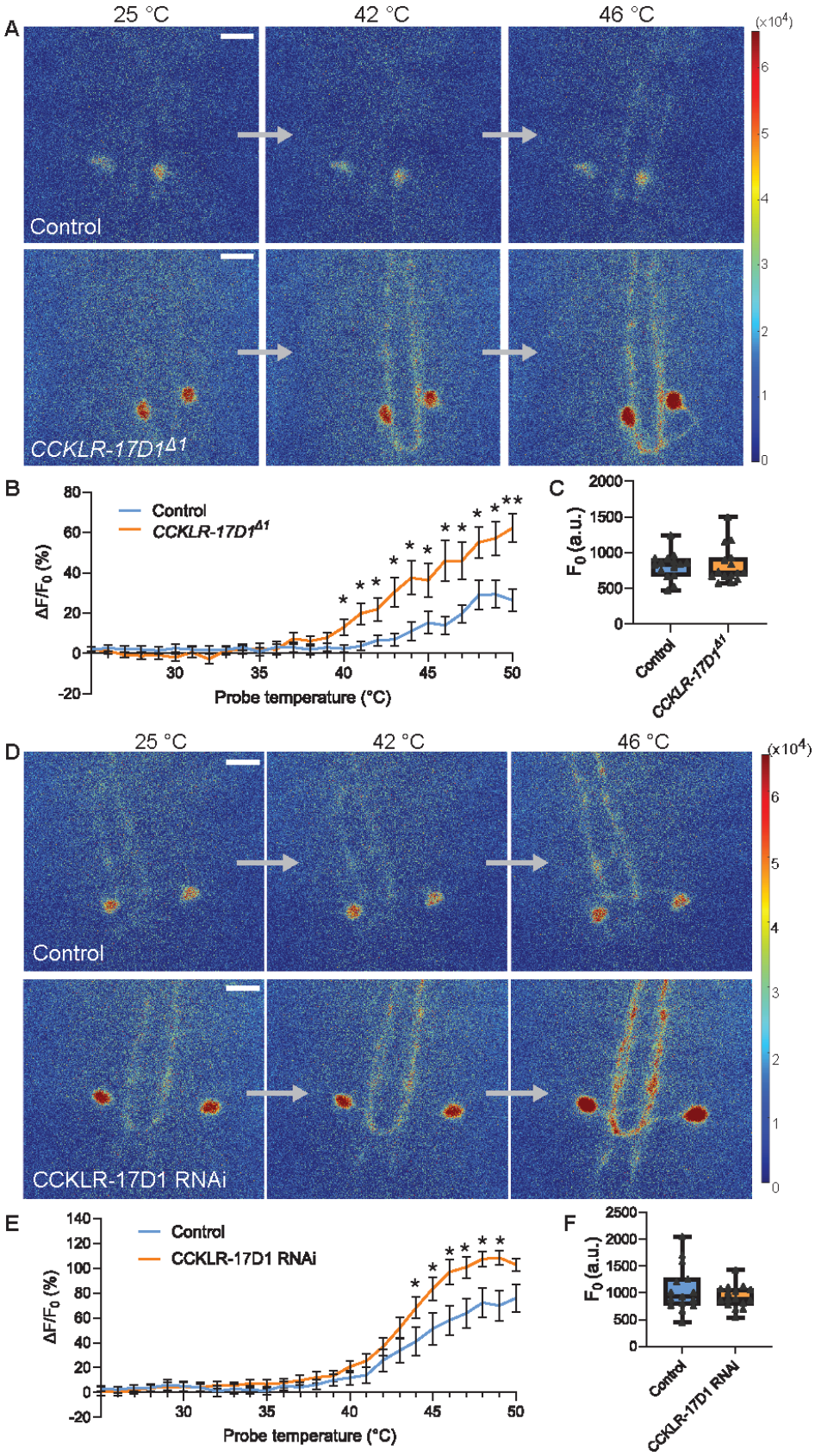
A
25 °C
42 °C
46 °C
(x10^4)
Control
CCKLR-17D1Δ1
B
Control
CCKLR-17D1Δ1
ΔF/F0 (%)
Probe temperature (°C)
C
F0 (a.u.)
Control
CCKLR-17D1Δ1
D
25 °C
42 °C
46 °C
(x10^4)
Control
CCKLR-17D1 RNAi
E
Control
CCKLR-17D1 RNAi
ΔF/F0 (%)
Probe temperature (°C)
F
F0 (a.u.)
Control
CCKLR-17D1 RNAi

415

416 **Figure 5. Goro neurons lacking CCKLR-17D1 show sensitized responses to noxious heat.**

417 (A) Representative still images showing thermal activation of Goro neurons in the controls (top, *yw*/Y; *R69E06-*

418 *GAL4 UAS-GCaMP6m/*+) and *CCKLR-17D1*$^{\Delta 1}$ mutants (bottom, *CCKLR-17D1*$^{\Delta 1}$*/Y; R69E06-GAL4 UAS-*

419 *GCaMP6m*/+). See also Video 1 and 2. (B) Average percent increase of GCaMP6m fluorescence intensity relative

420 to the baseline ($\Delta F/F_0$) during heat ramp stimulations in controls (n = 15) and *CCKLR-17D1*$^{\Delta 1}$ (n = 15). * $p < 0.05$,

421 ** $p < 0.01$ Mann-Whitney's U-test. (C) Basal GCaMP6m signal levels (F_0) in controls (n = 15) and *CCKLR-17D1*$^{\Delta 1}$

422 mutants (n = 15). $p > 0.6$ Mann-Whitney's U-test. (D) Representative stills showing thermal activation of the

423 controls (top, *R69E06-GAL4 UAS-GCaMP6m* x *yv; attp2*) and Goro neurons expressing CCKLR-17D1 RNAi

424 (bottom, *R69E06-GAL4 UAS-GCaMP6m* x *yv; JF02644*). See also Video 3 and 4. (E) Average percent increase of

425 GCaMP6m fluorescence intensity relative to the baseline ($\Delta F/F_0$) during heat ramp stimulations in controls (n = 15)

426 and CCKLR-17D1 RNAi (n = 16). * $p < 0.05$ Mann-Whitney's U-test. (F) Basal GCaMP6m levels (F_0) in controls

427 (n = 15) and CCKLR-17D1 RNAi (n = 16). $p > 0.6$ Mann–Whitney's U-test. Error bars represent standard error. All

428 box plots show median (middle line) and 25th to 75th percentiles with whiskers indicating the smallest to the largest

429 data points. All scale bars represent 20 µm.

430

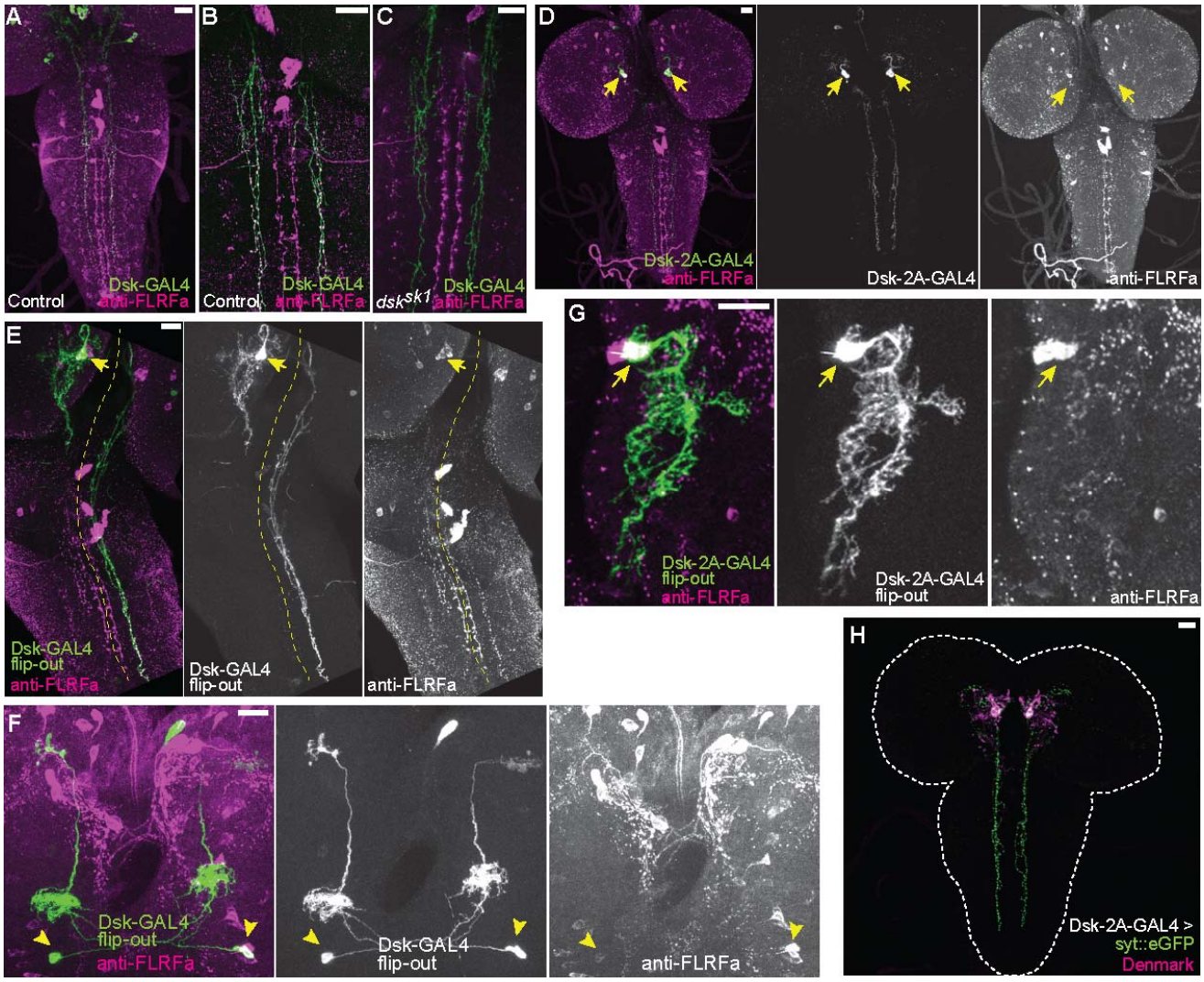

Figure 6. Projection patterns of DSK-expressing neurons in the larval CNS.

(A) Representative image showing descending axons from *DSK-GAL4* positive brain neurons (green) to the larval VNC. (B) Representative image showing all descending projections labeled by *DSK-GAL4* (green) harbor punctate anti-FLRFa signals (magenta) in the wild-type. (C) Representative image showing the complete absence of punctate anti-FLRFa signals (magenta) in the descending projections labeled by *DSK-GAL4* (green) in the dsk^{sk1} mutants. (D) Image showing the descending projections of MP1 neurons (arrows) marked by *DSK-2A-GAL4*. (E) Image

438 showing a single FLP-out clone of MP1 neuron (arrow) contralaterally sending descending axons to the larval VNC.

439 The yellow dashed line indicates the midline. (F) Image showing two FLP-out clones of Sv neurons (arrowheads)

440 sending ascending axons to both sides of the brain. (G) A projection image showing the MP1 neurites in the brain.

441 Note that few anti-FLRFa-positve puncta are associated with MP1 neurites within the brain. Similar expression

442 patterns were observed in multiple samples (n = 3). The arrow indicates the anti-FLRFa-positve MP1 soma. (H)

443 Representative image showing localizations of syt::eGFP (green) and Denmark (magenta) in MP1 neurons (*DSK-*

444 *2A-GAL4* x *UAS-syt::eGFP UAS-Denmark*). Similar expression patterns were observed in multiple samples (n =

445 7). All scale bars represent 20 μm.

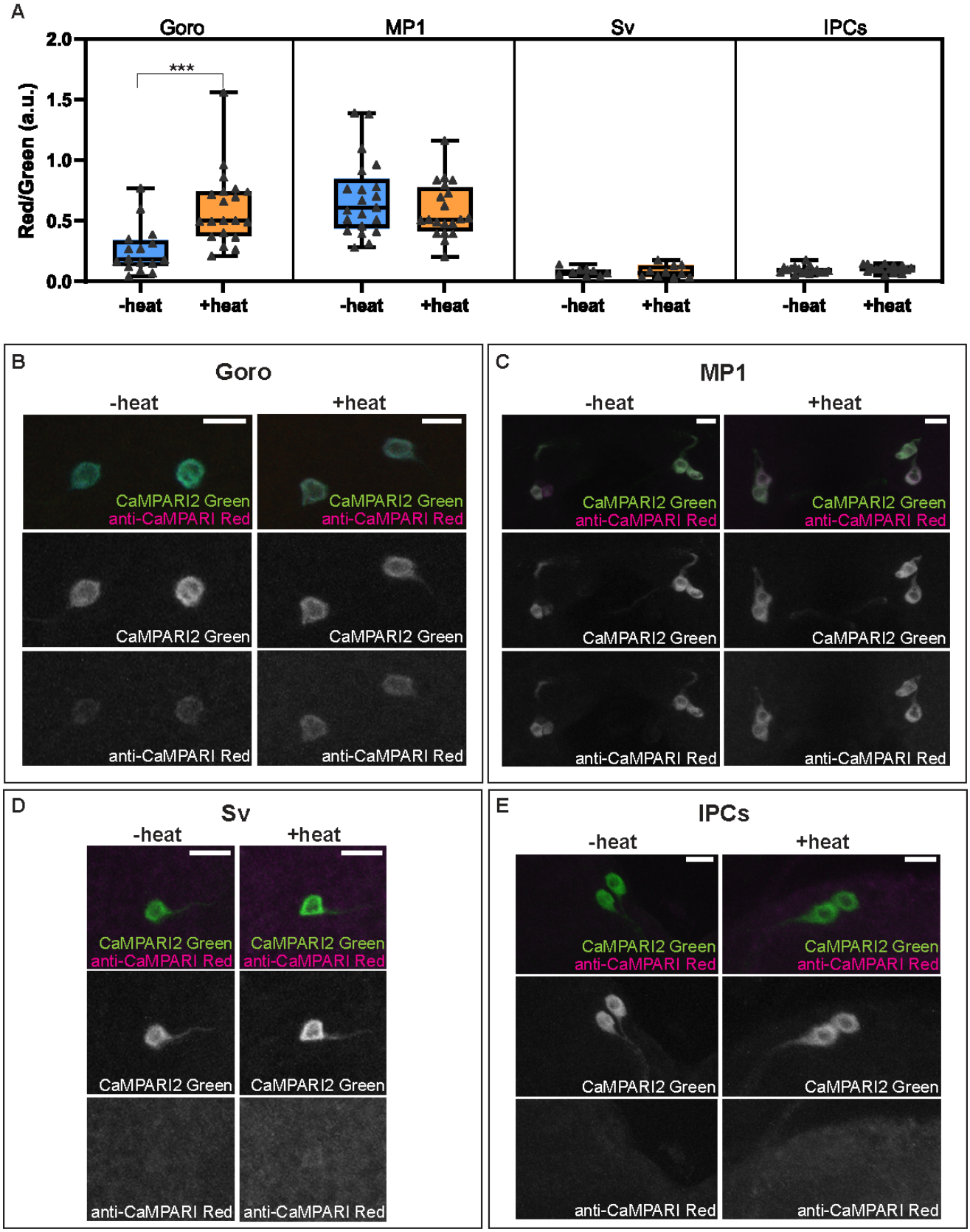
A
Goro
MP1
Sv
IPCs
Red/Green (a.u.)
2.0
1.5
1.0
0.5
0.0
***
-heat
+heat
B
Goro
C
MP1
D
Sv
E
IPCs
CaMPARI2 Green
anti-CaMPARI Red

446

447 **Figure 7. Activity and thermal responsiveness of DSK-expressing neurons.**

448 (A) Box plots of the quantified ratio of CaMPARI2 green signals and photoconverted CaMPARI2 red signals
449 detected by anti-CaMPARI-red in Goro, MP1, Sv, and IPCs (Red/Green) with or without local heat ramp stimulation.
450 Goro neurons showed a significantly higher Red/Green ratio of CaMPARI2 when local heat ramp stimulation was
451 applied to the larvae ($n = 16$ and 20, $p < 0.001$, Mann-Whitney's U-test). MP1 neurons showed a high Red/Green
452 ratio of CaMPARI2 both with and without local heat stimulation ($n = 21$ and 20, $p > 0.3$, Mann-Whitney's U-test).
453 The Red/Green ratio of CaMPARI2 was low in Sv compared to MP1 neurons, and CaMPARI2 photoconversion
454 was not increased by local heat stimulation ($n = 9$ and 10, $p > 0.5$, Mann-Whitney's U-test). IPCs also exhibited
455 low CaMPARI2 photoconversion regardless of the presence of local heat ramp stimulation ($n = 17$ and 16, $p > 0.25$,
456 Mann-Whitney's U-test). (B-E) Representative images showing CaMPARI2 green signals (green) and anti-
457 CaMPARI-red signals (magenta) in Goro (B), MP1 (C), Sv (D), and IPCs (E). All box plots show median (middle
458 line) and 25th to 75th percentiles, with whiskers indicating the smallest to the largest data points. Scale bars
459 represent 10 μm.

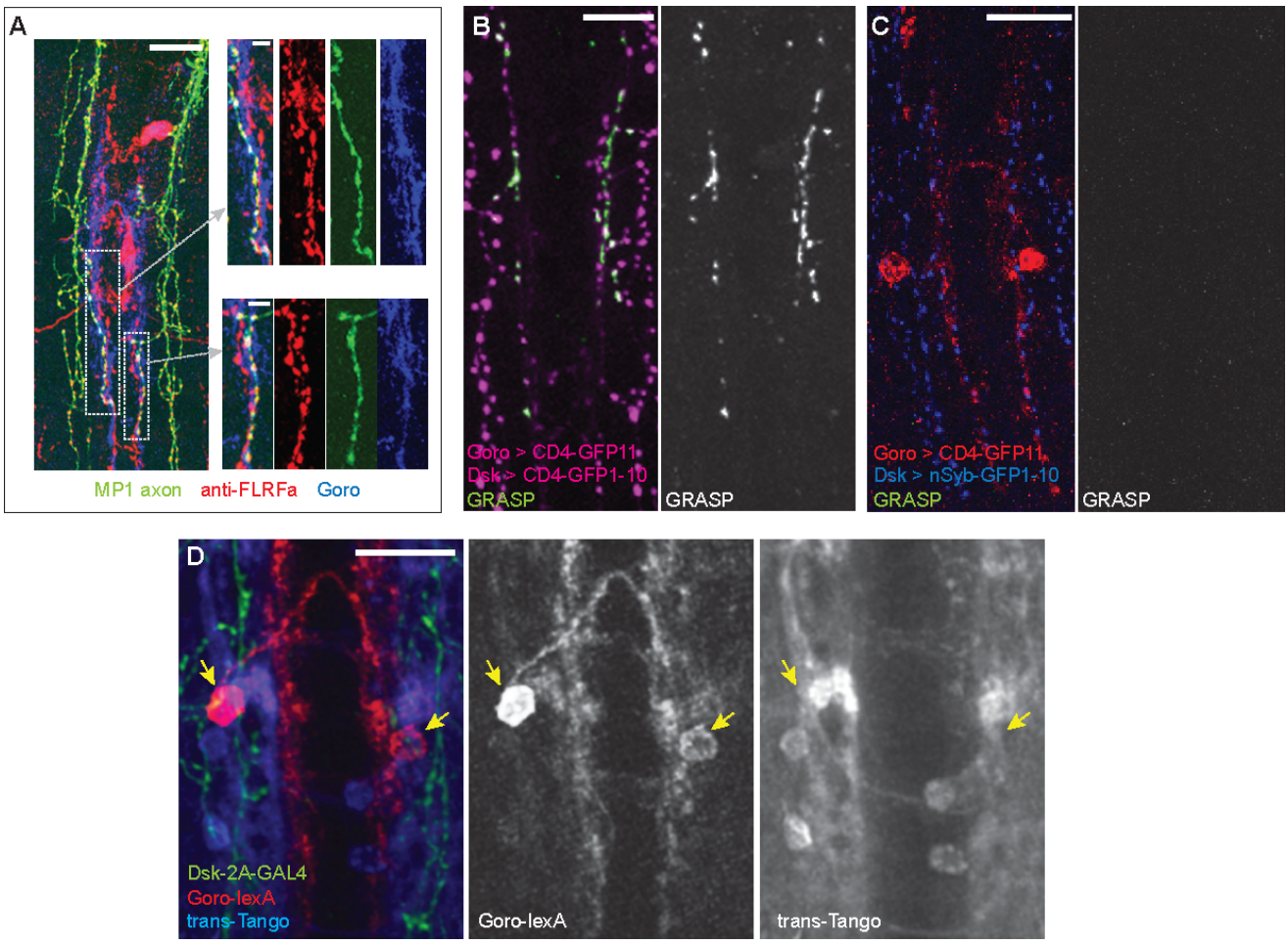

Figure 8. Synaptic connectivity between MP1 axons and Goro neurons is not detected.

(A) Representative images of the larval VNC showing partially overlapping MP1 axons (green) and processes of Goro neurons (blue) that are associated with anti-FLRFa signals (red). MP1 axons partially overlapping Goro neurons were similarly observed in all examined samples (n = 5). (B) Representative image showing CD4-GRASP experiments between MP1 axons and Goro neurons (magenta). Signals of reconstituted GFP (GRASP, green) were detected in all examined samples (n = 5). (C) Representative image showing nSyb-GRASP experiments between MP1 axons (blue) and Goro neurons (red). Signals of reconstituted GFP (GRASP, green) were not detectable in any

468 of the examined samples (n = 5). (D) Representative image showing *trans*-Tango experiments using *DSK-2A-GAL4*

469 (*R69E06-lexA, lexAop-rCD2::RFP UAS-mCD8::GFP; DSK-2A-GAL4* x *UAS-myrGFP, QUAS-mtdTomato::3xHA;*

470 *trans-Tango*). Transsynaptic activation of Tango signals (blue; mtdTomato::3xHA detected by anti-HA) was

471 undetectable in Goro neurons (red; rCD2::RFP detected by anti-CD2). Green represents MP1 axons labeled by

472 *DSK-2A-GAL4* (myrGFP and mCD8::GFP detected by anti-GFP). Signals of mtdTom::3xHA in Goro neurons were

473 not detected in any of the examined samples (n = 4). Arrows indicate Goro somata. All scale bars represent 20 µm,

474 except for the insets in (A) (5 µm).

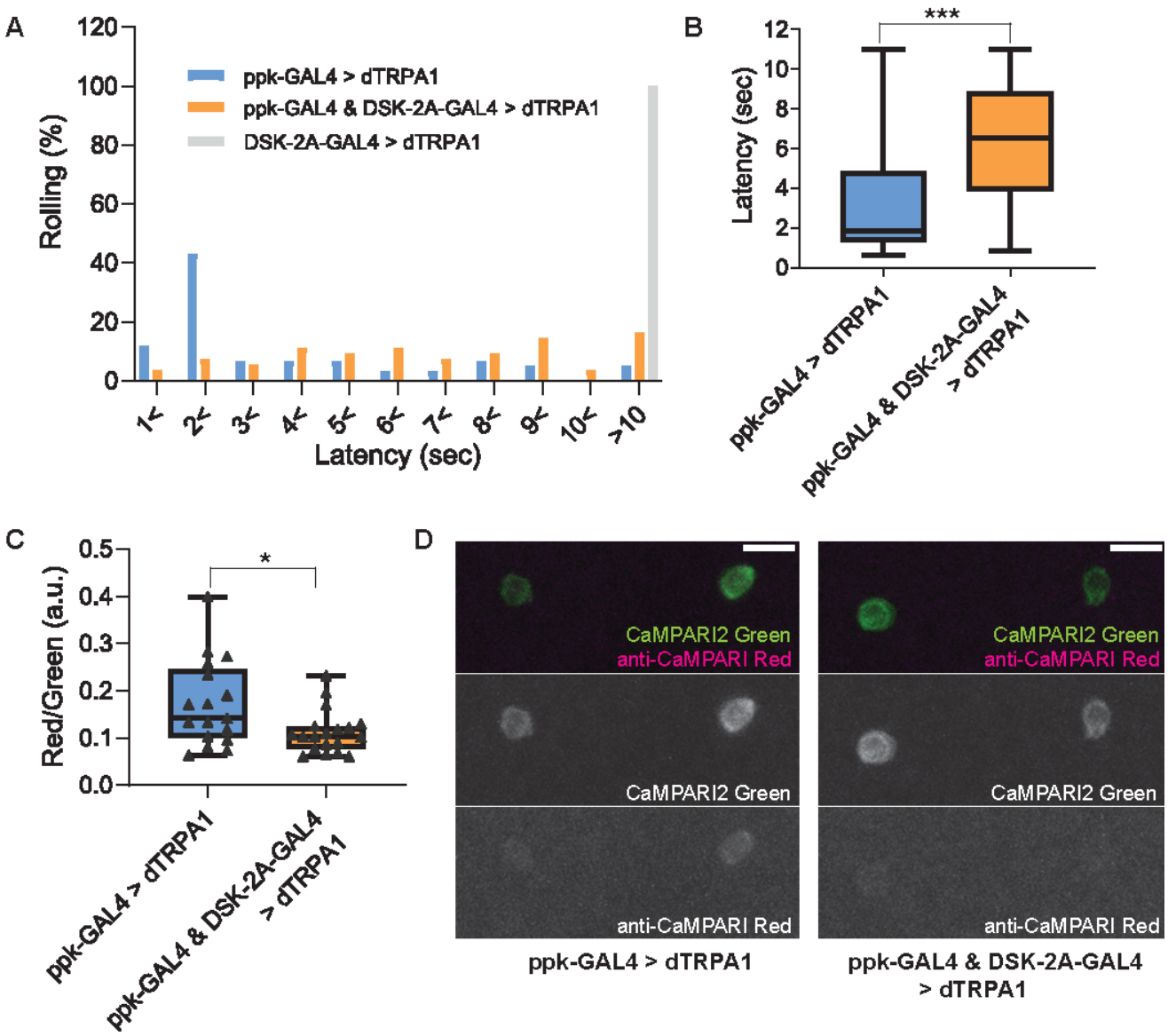

Figure 9. Thermogenetic activation of *DSK-2A-GAL4* neurons inhibits larval nociception and Goro neurons. (A and B) Thermogenetic activations of nociceptors and/or *DSK-2A-GAL4* neurons using *UAS-dTRPA1*. (A) Histogram representing the percentage of larvae exhibiting nociceptive rolling. Upon thermogenetic activations, 55% of larvae expressing dTRPA1 in nociceptors (ppk-GAL4 > dTRPA1; *ppk1.9-GAL4* x *UAS-dTRPA1*, n = 58)

481 exhibited nociceptive rolling within 2 seconds. In contrast, only 11% of larvae with simultaneous activations of
482 nociceptors and *DSK-2A-GAL4* showed rolling within 2 seconds (ppk-GAL4 & DSK-2A-GAL4 > dTRPA1; *ppk1.9-*
483 *GAL4 DSK-2A-GAL4* x *UAS-dTRPA1*, n = 54). Thermogenetic activations of *DSK-2A-GAL4* neurons alone (DSK-
484 2A-GAL4 > dTRPA1; *DSK-2A-GAL4* x *UAS-dTRPA1*, n = 40) did not trigger nociceptive responses even after 10
485 seconds. (B) Box plots showing latencies. Thermogenetic activation of *DSK-2A-GAL4* simultaneously with
486 nociceptors caused a significantly longer latency to rolling responses (Mann-Whitney U-test, *** $p < 0.001$). (C
487 and D) CaMPARI2 snapshot imaging of the activity of Goro neurons activated by thermogenetic stimulation of
488 C4da nociceptors. (C) Box plots of the ratio of CaMPARI2 green signals and photoconverted CaMPARI2 red signals
489 detected by anti-CaMPARI-red in Goro neurons (Red/Green). Compared to the larvae with thermogenetic activation
490 of C4da nociceptors only (ppk-GAL4 > dTRPA1; *ppk1.9-GAL4, UAS-dTRPA1* x *R69E06-lexA; lexAop-CaMPARI2*;
491 n = 17), the larvae with simultaneous activation of C4da and DSK-2A-GAL4 neurons (ppk-GAL4 & DSK-2A-
492 GAL4 > dTRPA1; *ppk1.9-GAL4, UAS-dTRPA1; DSK-2A-GAL4* x *R69E06-lexA; lexAop-CaMPARI2*; n = 19)
493 showed significantly decreased CaMPARI2 photoconversion in Goro neurons (Mann-Whitney U-test, * $p < 0.025$).
494 (D) Representative images showing CaMPARI2 green signals (green) and anti-CaMPARI-red signals (magenta) in
495 Goro neurons of animals with thermogenetic C4da activation (ppk-GAL4 > dTRPA1) and with simultaneous
496 thermogenetic activation of C4da and DSK-2A-GAL4 neurons (ppk-GAL4 & DSK-2A-GAL4 > dTRPA1). All box
497 plots show median (middle line) and 25th to 75th percentiles with whiskers indicating the smallest to the largest
498 data points. Scale bars represent 10 μm.

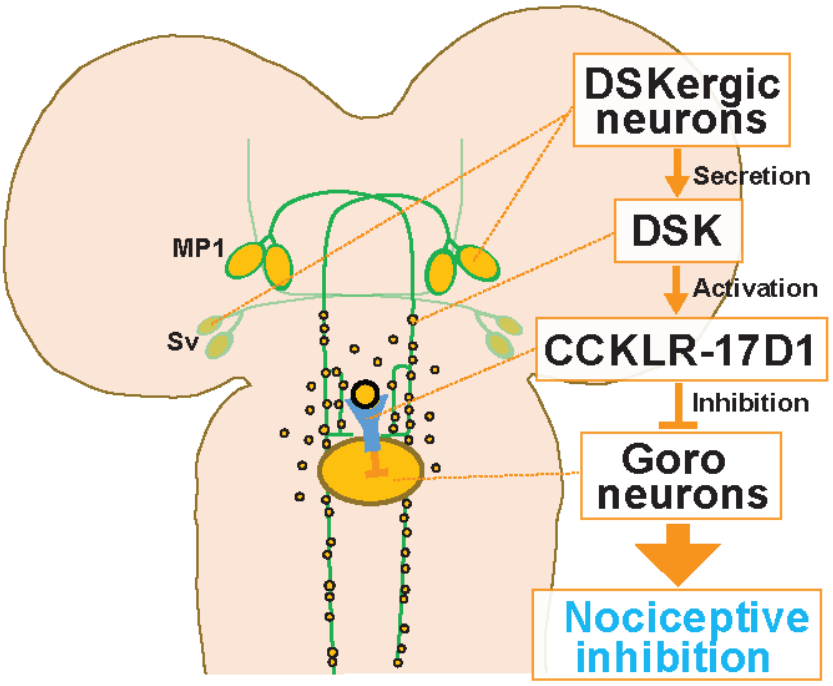

Figure 10. A schematic model of the DSKergic descending inhibitory pathway of nociception in larval *Drosophila*.

DSK-expressing MP1 and/or Sv neurons in the brain secrete DSK peptides. DSK in the larval VNC activates the CCKLR-17D1 receptor expressed in Goro neurons, which subsequently inhibits the activity of Goro neurons, and ultimately larval nociceptive rolling responses.

505 **Supplemental figures**

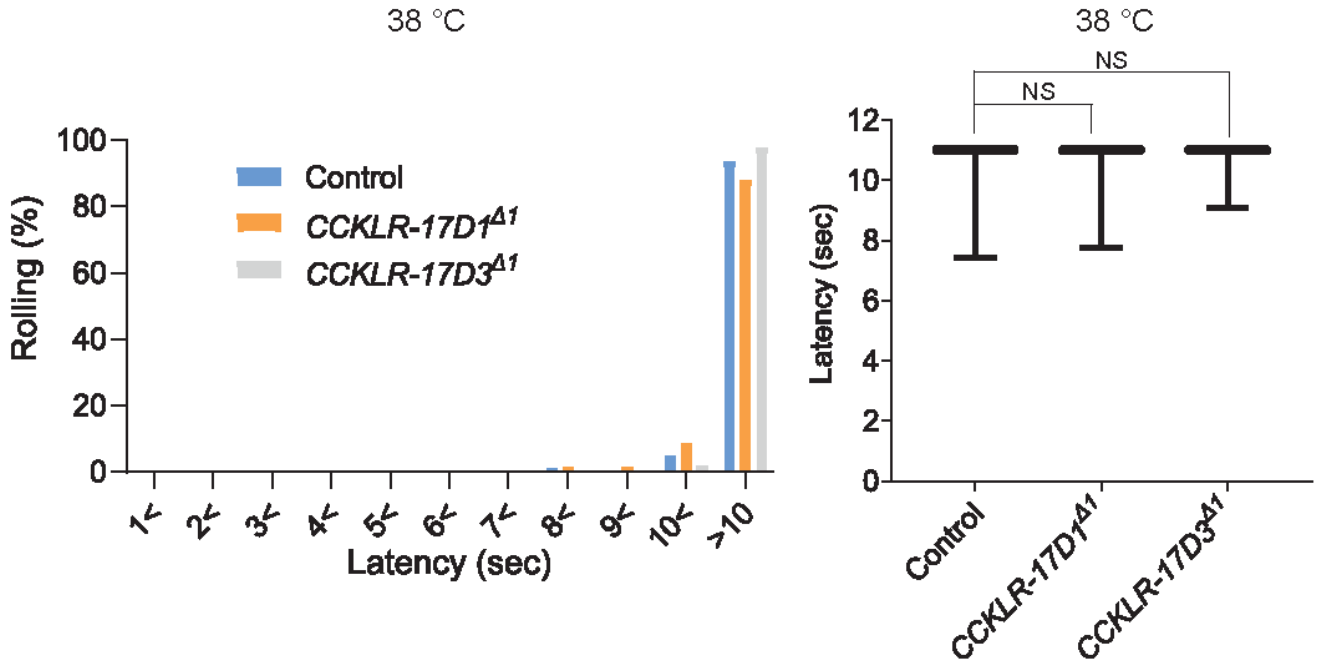

506

507 **Figure 1-figure supplement 1. Thermal nociceptive thresholds in DSK receptor mutants are largely normal.**

508 Thermal responses of *CCKLR-17D1* and *CCKLR-17D3* mutants to a 38 °C probe. Both *CCKLR-17D1*$^{\Delta 1}$ (n = 58)

509 and *CCKLR-17D3*$^{\Delta 1}$ (n = 48) showed comparable distributions of responding latencies to the controls (*yw*, n = 79).

510 Box plots show median (middle line) and 25th to 75th percentiles with whiskers indicating the smallest to the largest

511 data points. $p > 0.4$ Steel's test.

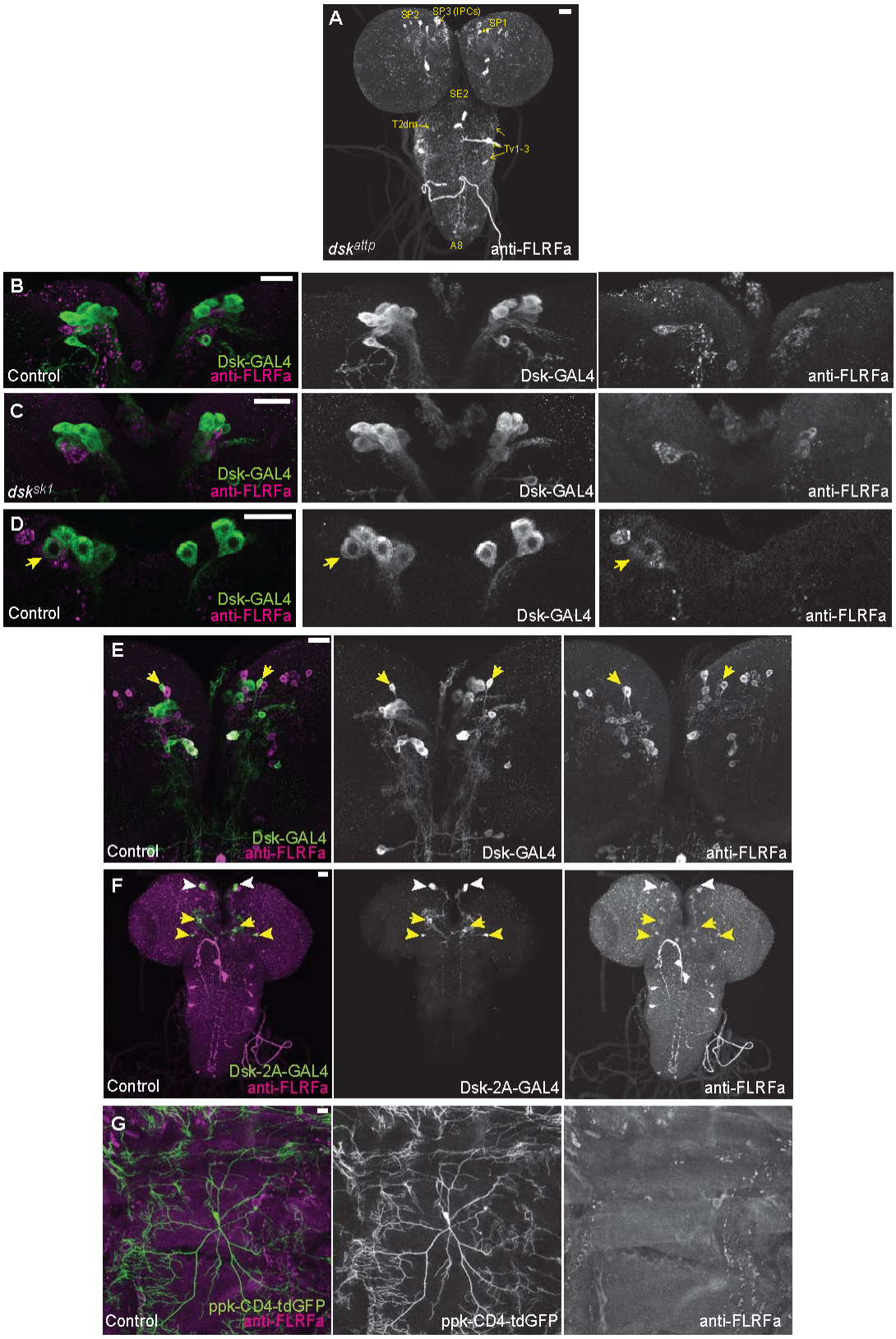
A
SP2
SP3 (IPCs)
SP1
SE2
T2drg
Tv1-3
A8
dsk^attp
anti-FLRFa
B
Control
Dsk-GAL4
anti-FLRFa
Dsk-GAL4
anti-FLRFa
C
dsk^sk1
Dsk-GAL4
anti-FLRFa
Dsk-GAL4
anti-FLRFa
D
Control
Dsk-GAL4
anti-FLRFa
Dsk-GAL4
anti-FLRFa
E
Control
Dsk-GAL4
anti-FLRFa
Dsk-GAL4
anti-FLRFa
F
Control
Dsk-2A-GAL4
anti-FLRFa
Dsk-2A-GAL4
anti-FLRFa
G
Control
ppk-CD4-tdGFP
anti-FLRFa
ppk-CD4-tdGFP
anti-FLRFa

512

513 **Figure 2-figure supplement 1. DSK expressions in the other brain neurons and peripheral sensory neurons.**

514 (A) Representative image showing staining of anti-FLRFa in *dsk*^{attp} mutants. The staining patterns were

515 indistinguishable from *dsk*^{sk1} mutants. (B) Representative image showing staining patterns of *DSK-GAL4* and anti-

516 FLRFa in the wild-type larval IPCs. In the wild-type brain, typically 4 to 7 IPCs are visualized by *DSK-GAL4* and

517 1 to 3 by anti-FLRFa consistently to the previous study by Soderberg et al. [49] that used anti-DSK raised by Nichols

518 et al. [47] In contrast, few IPCs co-labelled were found, which is also somewhat consistent with the variability of

519 DSK immunostaining in IPCs reported by the previous study [49]. (C) Representative image showing staining

520 patterns of *DSK-GAL4* and anti-FLRFa in the *dsk*^{sk1} larval IPCs. Comparable staining patterns of *DSK-GAL4* and

521 anti-FLRFa were observed in the mutant IPCs. (D) An example of rare IPC that was co-labeled by *DSK-GAL4* and

522 anti-FLRFa in the wild-type brain (arrow). (E) Representative image showing SP1 neurons (arrows) that were rarely

523 co-labeled by *DSK-GAL4* and anti-FLRFa. Note that faint anti-FLRFa staining was only detected in the SP1 neuron

524 in the right hemisphere. (F) An example image showing *DSK-2A-GAL4* expression in IPCs (white arrowheads),

525 MP1 (yellow arrows), and Sv neurons (yellow arrowheads). (G) Representative image showing double-labeling of

526 Class IV md neurons (*ppk-CD4::tdGFP*) and anti-FLRFa staining in the dorsal larval body wall. All scale bars

527 represent 20 μm.

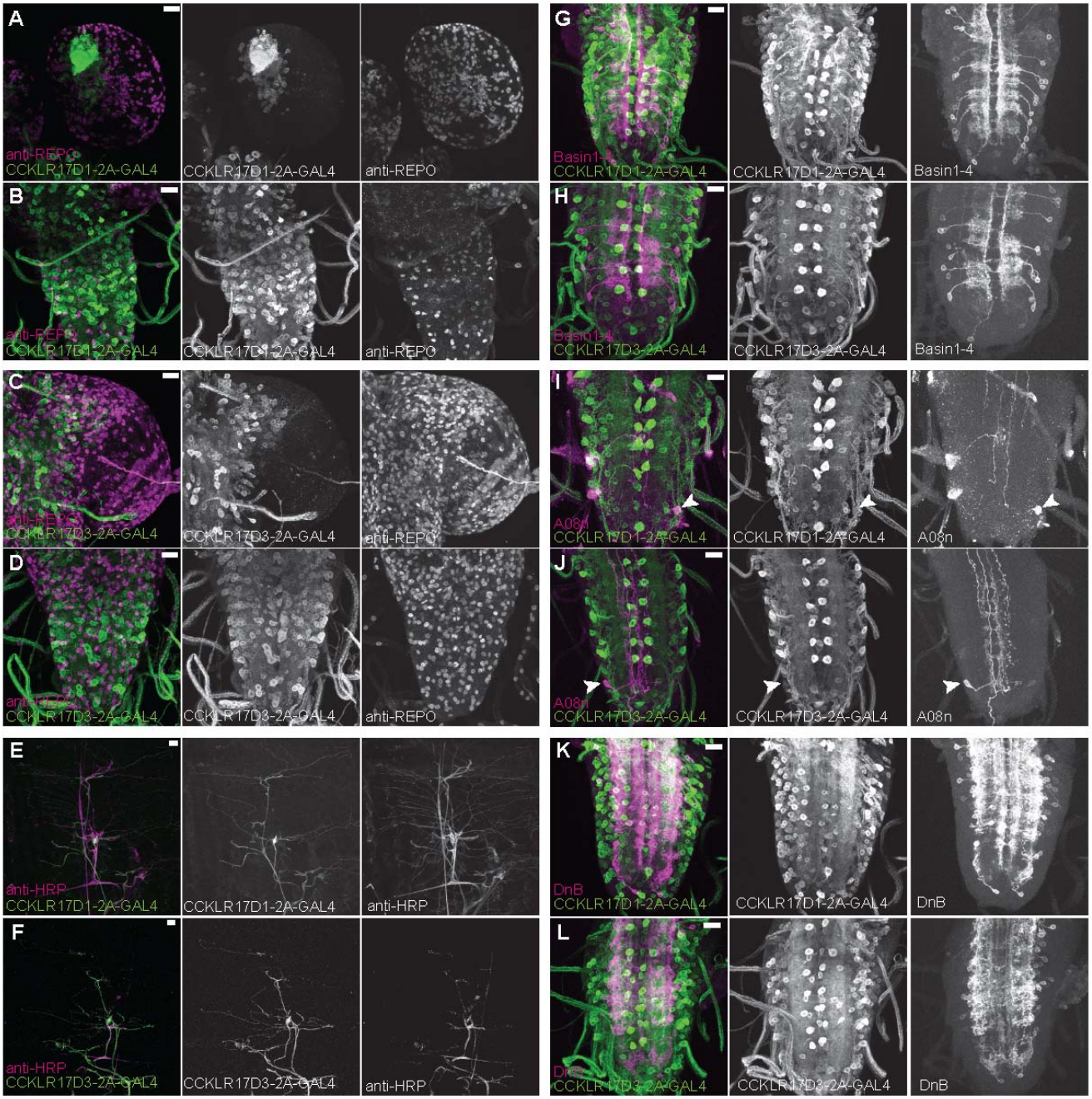

Figure 3-figure supplement 1. Expression patterns of DSK receptors in larval glial cells, peripheral tissue, and nociceptive interneurons.

(A and B) Representative images showing double-labeling of *CCKLR-17D1-T2A-GAL4* and a glial cell marker anti-

532 REPO in the larval brain (A) and the larval VNC (B), representing little expressions of *CCKLR-17D1-T2A-GAL4*
533 in glial cells. (C and D) Representative images showing double-labeling of *CCKLR-17D3-T2A-GAL4* and a glial
534 cell marker anti-REPO in the larval brain (C) and in the larval VNC (D), representing little expressions of *CCKLR-*
535 *17D3-T2A-GAL4* in glial cells. (E and F) Representative images showing the expressions of *CCKLR-17D1-T2A-*
536 *GAL4* (E) and *CCKLR-17D3-T2A-GAL4* (F) with a peripheral neuronal marker anti-HRP in the larval body wall,
537 showing the absence of both GAL4s from peripheral sensory neurons other than es cells. (G and H) Expressions of
538 *CCKLR-17D1-T2A-GAL4* (G) and *CCKLR-17D3-T2A-GAL4* (H) were negligible in Basin1 to 4 neurons labeled by
539 *R72F11-lexA* in the larval VNC. (I and J) Negligible expression of *CCKLR-17D1-T2A-GAL4* (I) and *CCKLR-17D3-*
540 *T2A-GAL4* (J) found in A08n neurons labeled by *R82E12-lexA* (arrowheads) in the larval VNC. (K and L)
541 Expressions of *CCKLR-17D1-T2A-GAL4* (K) and *CCKLR-17D3-T2A-GAL4* (L) were negligible in DnB neurons
542 labeled by *R70F01-lexA* in the larval VNC. All scale bars represent 20 μm.

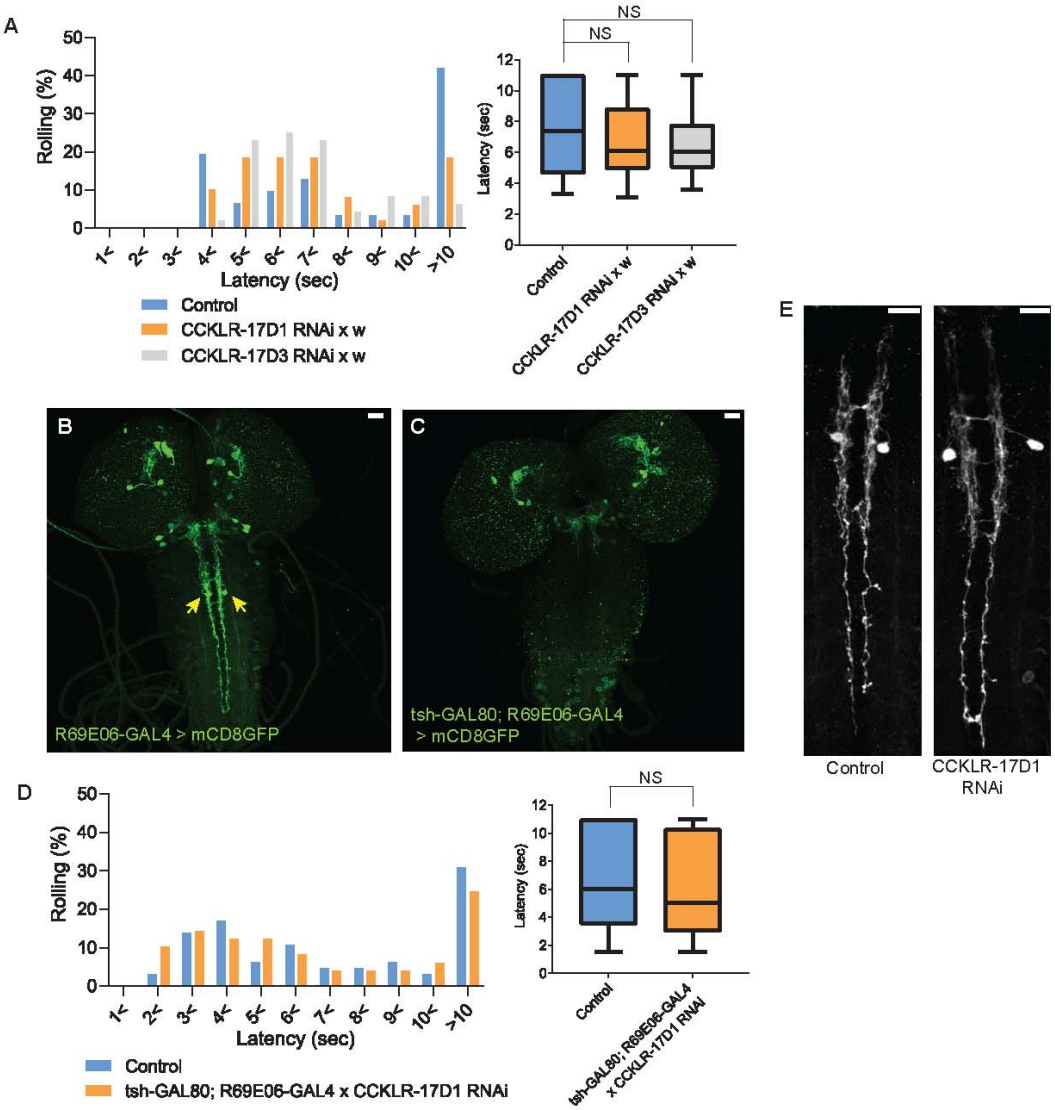

Figure 4-figure supplement 1. CCKLR-17D1 RNAi in Goro neurons induces thermal hypersensitivity in a GAL4-dependent manner, without affecting the morphology.

(A) Without the GAL4 driver, UAS-CCKLR-17D1 RNAi (*yv;JF02644* x w^{1118}, n = 49) and UAS-CCKLR-17D3 RNAi (*yv;JF02968* x w^{1118}, n = 48) both did not cause thermal hypersensitivity to 42 °C compared with the control (*R69E06-GAL4* x *yv; attp2,* n = 31). $p > 0.38$ Steel's test. (B and C) *tsh-GAL80* eliminates the expression of *R69E06-*

549 *GAL4* from Goro neurons. The expression of *R69E06-GAL4* in Goro neurons (B) (*10xUAS-IVS-mCD8GFP;*

550 *R69E06-GAL4* x *yv; attp2*) was eliminated when *tsh-GAL80* was combined with *R69E06-GAL4* (C) (*tsh-GAL80;*

551 *R69E06-GAL4* x *40xUAS-IVS-mCD8GFP*). (D) When the expression of UAS-CCKLR-17D1 RNAi was eliminated

552 from Goro neurons (*tsh-GAL80; R69E06-GAL4* x *yv; JF02644*, n = 49), larval nociceptive responses to a 42 °C

553 probe was indistinguishable from the control (*R69E06-GAL4* x *yv; attp2,* n = 65). $p > 0.33$ Mann-Whitney's U-test.

554 (E) Goro neurons expressing CCKLR-17D1 RNAi (*10xUAS-IVS-mCD8GFP; R69E06-GAL4* x *yv; JF02644*) did

555 not alter their number, position, and gross projection patterns in comparison with the control (*10xUAS-IVS-*

556 *mCD8GFP; R69E06-GAL4* x *yv; attp2*). All scale bars represent 20 µm. All box plots show median (middle line)

557 and 25th to 75th percentiles with whiskers indicating the smallest to the largest data points.

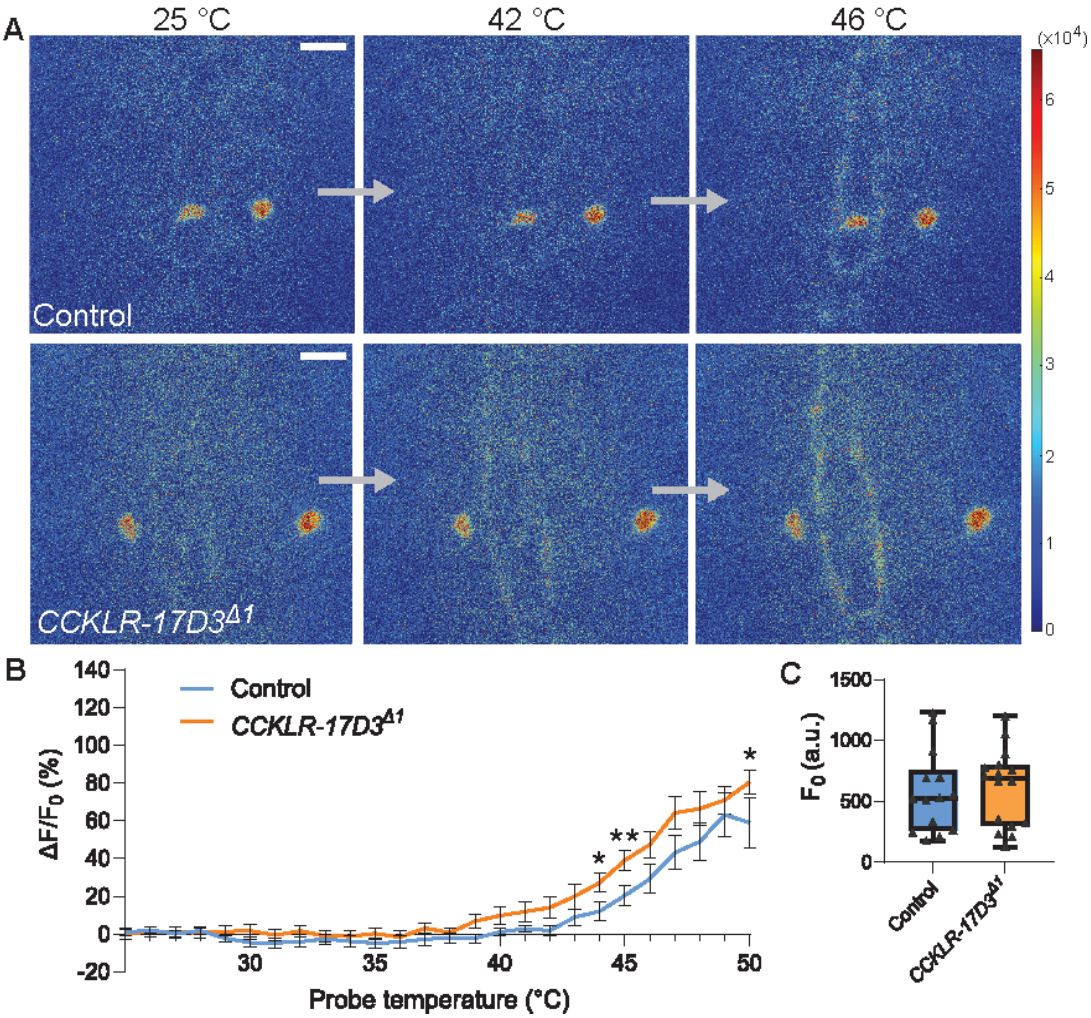

558

559 **Figure 5-figure supplement 1. Thermal responsiveness of Goro neurons in CCKLR-17D3Δ1.**

560 (A) Representative still images showing thermal activation of Goro neurons in control animals (top, *yw*/Y; *R69E06-*

561 *GAL4 UAS-GCaMP6m/+*) and *CCKLR-17D3*$^{\Delta 1}$ mutants (bottom, *CCKLR-17D3*$^{\Delta 1}$*/Y; R69E06-GAL4 UAS-*

562 *GCaMP6m/+*). See also Movie S5 and S6. Scale bars represent 20 µm. (B) Average percent increase of GCaMP6m

563 fluorescence intensity relative to baseline ($\Delta F/F_0$) during heat ramp stimulations in *CCKLR-17D3*$^{\Delta 1}$ experiments.

564 $\Delta F/F_0$ is plotted to binned probe temperature (interval = 1 °C). In comparison with controls, Goro neurons of

565 *CCKLR-17D3*$^{\Delta 1}$ exhibited mildly elevated fluorescent increase of GCaMP6m, which reached statistical significance

566 only at 44°C, 45°C, and 50°C. n = 14 and 16 for controls and *CCKLR-17D3*$^{\Delta 1}$, respectively. * $p < 0.05$, ** $p < 0.01$

567 (Mann–Whitney's U-test). Error bars represent standard errors. (C) Basal GCaMP6m signal levels (F_0) did not differ

568 between controls and *CCKLR-17D3*$^{\Delta 1}$ (n = 14 and 16). $p > 0.5$ (Mann–Whitney's U-test). Box plots show median

569 (middle line) and 25th to 75th percentiles with whiskers indicating the smallest to the largest data points.

570 **Video 1.**

571 Ca2+ imaging of Goro neurons in a control animal used for the CCKLR-17D1Δ1 experiments. See also Figure 5.

572 The movie was generated from heat-mapped time-series projection images of GCaMP6m fluorescence using

573 MATLAB. Time and probe temperature are indicated at the top left and top right corners, respectively.

574

575 **Video 2.**

576 Ca2+ imaging of Goro neurons in a CCKLR-17D1Δ1 mutant animal. See also Figure 5. The movie was generated

577 from heat-mapped time-series projection images of GCaMP6m fluorescence using MATLAB. Time and probe

578 temperature are indicated at the top left and top right corners, respectively.

579

580 **Video 3.**

581 Ca2+ imaging of Goro neurons in a control animal used for the CCKLR-17D1 RNAi experiments. See also Figure

582 5. The movie was generated from heat-mapped time-series projection images of GCaMP6m fluorescence using

583 MATLAB. Time and probe temperature are indicated at the top left and top right corners, respectively.

584

585 **Video 4.**

586 Ca2+ imaging of Goro neurons in a CCKLR-17D1 RNAi animal. See also Figure 5. The movie was generated from

587 heat-mapped time-series projection images of GCaMP6m fluorescence using MATLAB. Time and probe

588 temperature are indicated at the top left and top right corners, respectively.

589

590 **Video 5.**

591 Ca2+ imaging of Goro neurons in a control animal used for the CCKLR-17D3Δ1 experiments. See also Figure 5-

592 figure supplement 1. The movie was generated from heat-mapped time-series projection images of GCaMP6m

593 fluorescence using MATLAB. Time and probe temperature are indicated at the top left and top right corners,

594 respectively.

595

596 **Video 6.**

597 Ca2+ imaging of Goro neurons in a CCKLR-17D3Δ1 mutant animal. See also Figure 5-figure supplement 1. The

598 movie was generated from heat-mapped time-series projection images of GCaMP6m fluorescence using MATLAB.

599 Time and probe temperature are indicated at the top left and top right corners, respectively.

600

601

602 **Figure 1-source data 1.**

603 Source data used to generate the summary data and graphs shown in Figure 1 and Figure 1-figure

604 supplement 1.

605

606 **Figure 4-source data 1.**

607 Source data used to generate the summary data and graphs shown in Figure 4 and Figure 4-figure

608 supplement 1.

609

610 **Figure 5-source data 1.**

611 Source data used to generate the summary data and graphs shown in Figure 5 and Figure 5-figure

612 supplement 1.

613

614 **Figure 7-source data 1.**

615 Source data used to generate the summary data and graphs shown in Figure 7.

616

617 **Figure 9-source data 1.**

618 Source data used to generate the summary data and graphs shown in Figure 9.

619

620 **Materials and Methods**

621 **Fly strains**

622 *y^1w^{1118}* strain was used as the control strain for *dsk*, *CCKLR-17D1*, and *CCKLR-17D3* mutants. *yv*; attp2 strain was

623 used for the control of *yv; JF02644* (CCKLR-17D1 RNAi) and *yv; JF02968* (CCKLR-17D3 RNAi). *yw; nos-*

624 *Cas9/CyO* (NIG-FLY CAS-0011) and *yw; Pr Dr/TM6C Sb Tb* were used for CRISPR/Cas9 mutagenesis. *Dp(3;1)2-*

625 *2, w^{1118}; Df(3R)2-2/TM3 Sb* (Bloomington #3688), *UAS-CCKLR-17D1* (66), and *UAS-CCKLR-17D3* (this study)

626 were used for rescue experiments. *DSK-GAL4* (Bloomington #51981), *DSK-2A-GAL4* (Bloomington #84630),

627 *R69E06-GAL4* (Bloomington #39493), *R69E06-lexA* (Bloomington #54925), *R72F11-lexA* (53), *R70F01-lexA*

628 (Bloomington #53628), *R38A10-lexA* (Bloomington #54106), *R82A10-lexA* (Bloomington #54417), *CCKLR-17D1-*

629 *T2A-GAL4* (79), *CCKLR-17D3-T2A-GAL4* (79) and *tsh-GAL80* were used for tissue-specific gene expressions.

630 *40xUAS-IVS-mCD8::GFP* (Bloomington #32195), *10xUAS-IVS-mCD8GFP* (Bloomington #32186), *UAS>CD2*

631 *stop>mCD8::GFP hs-flp* (80), *lexA-rCD2::RFP UAS-mCD8::GFP* (81), *ppk-CD4::tdGFP* (Bloomington #35842),

632 *UAS-nSyb-GFP_{1-10}; lexAop-CD4-GFP_{11}* (Bloomington #64314), *UAS-CD4-GFP_{1-10}; lexAop-CD4-GFP_{11}*

633 (Bloomington #58755), *UAS-Denmark UAS-syt::eGFP* (Bloomington #33065), and *UAS-myrGFP QUAS-*

634 *mtdTomato::3xHA; trans-Tango* (Bloomington #77124) were used for cellular visualizations. *UAS-GCaMP6m*

635 (Bloomington #42748) was used for GCaMP Ca^{2+} imaging. *UAS-dTRPA1* (Bloomington #26263) (64) was used for

636 thermogenetic experiments. , *UAS-CaMPARI2* (Bloomington #78316) and *lexAop-CaMPARI2* (Bloomington

637 #78325) were used for CaMPARI2 snapshot imaging of neuronal activity. *dsk^{sk1}*, *CCKLR-17D1* deletion mutants,

638 *CCKLR-17D3* deletion mutants, and *UAS-CCKLR-17D3* were generated in this study and described below. *dsk*^{attp}

639 strain (52) was obtained from the Bloomington stock center (#84497). Stocks were kept at 25°C with 12:12 hour

640 light cycle on a standard food.

641 **Generating mutants and transgenic lines**

642 Deletion mutants of *dsk*, *CCKLR-17D1,* and *CCKLR-17D3* were generated as described previously (82). Briefly,

643 23 bp-guide RNA (gRNA) sequences specific to the aimed region of the targeted genes were identified using an

644 online tool (http://www.flyrnai.org/crispr/) and 20-bp sequences excluding PAM were cloned to the pBFv-U6.2

645 vector. Injections of the gRNA-pBFv-U6.2 vectors to yield transgenic fly strains were performed by BestGene Inc.

646 The gRNA-expressing lines were crossed with a nos-Cas9 strain and about 20 independent F1 generations that

647 could potentially possess modifications in the targeted genomic region were established. Lines that had a

648 frameshifting deletion in the targeted region were screened through standard PCR and sequencing. The following

649 gRNA and PCR primer sequences were used to generate *dsk*, *CCKLR-17D1*, and *CCKLR-17D3* mutants:

650 ● *dsk*: GTAGACTAGTCGTCTGCGCT (gRNA), CCTCTAAACACTTGACAGCCGCGGTAACGG (forward

651 primer), and CCGAAACGCATGTGACCGTAGTCATCG (reverse primer).

652 ● *CCKLR-17D1*: GCTTCCGTGATACGCAGACTGGG (gRNA), ATGTGTTTTGTGGATACCCTGT (forward

653 primer), and GGGCTATACCTCCA-TCAGTTTC (reverse primer).

654 ● *CCKLR-17D3*: GCCATATCGGACATGCTGCTGGG (gRNA), GATAGGGA-

655 TGGCTATATGGACACCGAGC (forward primer), and CTTAGCTGTCCCAATTCCCCCATCTTCT (reverse

656 primer).

657 The UAS-CCKLR-17D3 line was generated through a ΦC31 integrase–based method. The oligo DNA
658 corresponding to the sequence of CCKLR-17D3 mRNA (+447-2201 of AY231149) was synthesized (Eurofins
659 Genomics) and cloned into the pUASg.attB vector (83) using the pENTR/D-TOPO Gateway cloning kit (Thermo
660 Fisher Scientific, MA). The sequence-verified UAS-CCKLR-17D3 construct was integrated into the attP40 site to
661 yield transgenic lines. The injections were performed by BestGene Inc.

662 **Thermal nociception assay**

663 The experimenters were blinded to genotypes. Larval thermal nociception assays were performed as described
664 previously (31), with slight modifications. A custom-made probe with a thermal feedback system was used. Unless
665 otherwise noted, a thermal probe heated to 42°C was used to detect hypersensitive phenotypes (32). The results
666 from all non-responders, defined as individuals that did not exhibit rolling behavior within 10 seconds, were
667 converted to data points of 11 seconds for subsequent statistical analyses.

668 **Thermogenetic activation experiments**

669 The experimenters were blinded to genotypes. A 60 mm dish containing approximately 1 ml distilled water (testing
670 chamber) was placed on a temperature-controlled plate MATS-SPE (TOKAI HIT, Shizuoka, Japan) set at 44.5 °C
671 to equilibrate the water temperature in a testing chamber to 35 ± 1 °C, which was continuously monitored using a
672 T-type thermocouple wire IT-23 (Physitemp, NJ), USB-TC01 (National Instruments), and the NI Signal Express
673 software (National Instruments, TX). Wandering third instar larvae expressing dTRPA1 by *ppk1.9-GAL4* and/or

674 *DSK-2A-GAL4* were harvested to another 60 mm dish at room temperature (23-25 °C), and gently transferred to the
675 35 °C testing chamber using a paintbrush. All experiments were performed and recorded under a binocular
676 microscope with a camcorder, and the latency from the placement of larvae to rolling was measured offline for each
677 larva.

678 **Immunohistochemistry**

679 The following antibodies were used in this study: chicken anti-GFP (Abcam, 1:500), mouse anti-GRASP (Sigma
680 #G6539, 1:100) (62), mouse anti-rat CD2 (Bio-Rad, 1:200), rat anti-mCD8 (Caltag, 1:100), rabbit anti-FLRFa (a
681 gift from Dr. Eve Marder, 1:5000) (84), rabbit anti-CD4 (Novus Biologicals, 1:500), mouse anti-REPO
682 (Developmental Studies Hybridoma Bank 8D12, 1:5), rabbit anti-DsRed (Clontech #632496, 1:200), rat anti-HA
683 (Roche 3F10, 1:100), mouse anti-CaMPARI-red (Absolute antibody 4F6, 1:1000), goat anti-HRP-Cy3 (Jackson
684 ImmunoResearch, 1:100), goat anti-rat Alexa488 (Invitrogen, 1:500), goat anti-chicken Alexa488 (Invitrogen,
685 1:500), goat anti-mouse Alexa546 (Invitrogen, 1:500), goat anti-rabbit Alexa546 (Invitrogen, 1:500), goat anti-rat
686 Alexa633 (Invitrogen, 1:500), and goat anti-rabbit Alexa633 (Invitrogen, 1:500). Dissected larval tissues were fixed
687 in 4% paraformaldehyde for 30 minutes and then stained as previously described (32). The images were acquired
688 by using a Zeiss LSM 510 with a 20x/0.75 Plan-Apochromat objective or 40x/1.0 Plan-Apochromat oil immersion
689 objective, Zeiss LSM 700 with a 20x/0.75 Plan-Apochromat objective or 40x/1.0 Plan-Apochromat oil immersion
690 objective, or Leica SP5 with a 40x/0.85 PL APO objective, and digitally processed using Zeiss LSM Image Browser,
691 Leica LAS X Lite, and Adobe Photoshop.

692 **GRASP and *trans*-Tango experiments**

693 The CD4-GRASP experiments were performed by crossing the *R69E06-lexA DSK-GAL4* strain with the *UAS-CD4-*
694 *GFP$_{1-10}$; lexAop-CD4-GFP$_{11}$*. The nSyb-GRASP experiments were performed by crossing the *R69E06-lexA DSK-*
695 *GAL4* with the *UAS-nSyb-GFP$_{1-10}$; lexAop-CD4-GFP$_{11}$*. Wandering 3rd instar larvae were dissected and
696 immunostained as mentioned above. The signals of the reconstituted GFP were detected using a GFP antibody
697 without cross-reaction to split-GFP fragments (Sigma #G6539) (62).

698 The *trans*-Tango experiments were performed by crossing the *R69E06-lexA, lexAop-rCD2::RFP UAS-*
699 *mCD8::GFP; DSK-2A-GAL4* with *UAS-myrGFP QUAS-mtdTomato::3xHA; trans-Tango*. Wandering 3rd instar
700 larvae were dissected and immunostained as mentioned above. The following combinations of the primary and
701 secondary antibodies were used to avoid cross-contamination of fluorescent signals in microscopy: chick anti-GFP
702 and anti-chick Alexa488, mouse anti-rCD2 and anti-mouse Alexa546, and rat anti-HA and anti-rat Alexa633.

703 **FLP-out clone analysis**

704 The *UAS>CD2 stop>mCD8::GFP hs-flp* strain was crossed with *DSK-GAL4* or *DSK-2A-GAL4* to seed vials. Heat-
705 shock induction of FLP-out clones and immunostaining were performed as described previously (32). The images
706 of brain samples were acquired and digitally processed as described above.

707 **GCaMP calcium imaging**

708 Ca^{2+} imaging of Goro neurons using GCaMP6m (85) was performed as described previously (32), with some
709 modifications. Wandering third instar larvae expressing GCaMP6m in Goro neurons by *R69E06-GAL4* were

710 dissected in ice-cold hemolymph-like saline 3.1 (HL3.1) (86) and imaged in a custom-made imaging chamber
711 containing the HL3.1 equilibrated to the room temperature (23-25 °C). A Leica SP8 confocal microscope with
712 resonant scanning system was used to perform three-dimensional time-lapse imaging. Z-stacks consisting of 4 to 6
713 optical slices of 512 x 512 pixel images were acquired at approximately 0.5 to 1 Hz using a 10x/0.4 PL APO
714 objective lens with a zoom factor of 8.0. During imaging, a local heat ramp stimulation was applied to the lateral
715 side of the A5 to A7 segment with a custom-made thermal probe. The probe temperature was controlled using a
716 Variac transformer set at 20 V, which generated an approximately 0.6 °C/sec heat ramp stimulus. A T-type
717 thermocouple wire was placed inside of the thermal probe to acquire the probe temperature readings and the data
718 were acquired at 4 Hz through a digitizer USB-TC01 (National Instruments) and the NI Signal Express software
719 (National Instruments). To minimize potential biases caused by day-to-day variations in imaging conditions and
720 achieve fair comparisons, similar numbers of control and experimental genotypes were imaged side-by-side on the
721 same day, using identical microscope settings. To monitor the temperature around the larval CNS during the local
722 heat ramp stimulation, a small thermocouple wire (IT-23, Physitemp) was placed nearby the exposed CNS of semi-
723 dissected larvae.

724 Maximum intensity projections were generated from the time-series Z-stacks on Leica LAS X Lite and
725 the subsequent analyses of the images and temperature log data were performed using a custom-made code in
726 MATLAB (MathWorks, MA). The region of interest (ROI) was selected as a circular area with a diameter of 15
727 pixels that covered the neurites of Goro neurons. Cell bodies were not used for the quantification because of small

728 and variable increases in GCaMP6m signals upon heat stimulation. Average fluorescent intensity (F) was calculated

729 for the ROI for each time point. The average of Fs from the first five frames was used as the baseline fluorescent

730 intensity (F_0) and percent changes of fluorescent intensity from the baseline [$\Delta F/F_0 = (F - F_0)*100/F_0$] was calculated

731 for each time point. At least three ROIs were selected from areas that were expected to yield high GCaMP6m signal

732 increases and the ROI that led to the highest peak $\Delta F/F_0$ was chosen for the subsequent statistical analysis. Samples

733 whose highest peak $\Delta F/F_0$ was less than 10% were excluded from the analysis to avoid potential skewness of the

734 data by inclusion of dead/unhealthy samples. Because the images and probe temperatures could not be acquired at

735 the same time, probe temperature for each time point was calculated by linear interpolation from the raw readings.

736 For comparisons among strains, $\Delta F/F_0$ data were binned and averaged in 1 °C intervals.

737 **CaMPARI2 experiments**

738 Wandering third instar larvae expressing CaMPARI2 with *R69E06-GAL4* or *DSK2A-GAL4* were harvested from

739 vials to a 60-mm petri dish and rinsed with water. Each larva was transferred onto kimwipe to remove moisture and

740 attached with its ventral side up on labeling tape. A custom-made thermal probe (the same probe described for

741 GCaMP experiments above) was placed at the lateral side of the A5 to A7 segment, and a local thermal ramp

742 stimulus from room temperature (23-25 °C) to 50 °C was applied using a Variac transformer set at 20 V.

743 Simultaneously with local heat ramp stimulation, 405 nm UV light was applied from 3 cm above the animal using

744 a 405nm LED stand light (7 mW/cm^2, LED405-9VIS, OPTOCODE Corporation, Tokyo, Japan). In "no heat"

745 control experiments, no voltage was applied to the thermal probe attached to the larva, and only 405 nm light

746 irradiation was applied for 40 seconds (equivalent to the length of time required to apply a temperature ramp
747 stimulus from room temperature to 50°C with 20 V). In thermogenetic activation experiments, larvae expressing
748 CaMPARI2 under the control of *R69E06-lexA* and dTRPA1 under the control of either only *ppk1.9-GAL4* or both
749 *ppk1.9-GAL4* and *DSK-2A-GAL4* were immobilized on labeling tape with their ventral side up. The larvae were
750 then transferred onto a MATS-SPE temperature-controlled plate set at 35 °C, and simultaneously irradiated with
751 405 nm light for 10 seconds from 3 cm above.

752 Immediately after thermal stimulation and/or photoconversion, the larvae were gently rinsed with water,
753 removed from the labeling tape, and pooled into a new 60-mm dish. Five to fifteen animals were pooled for each
754 experimental group and dissected immediately in ice-cold PBS. The larval CNS samples were immunostained
755 following the protocol described above with mouse anti-CaMPARI red (4F6), rat anti-HA (3F10), anti-mouse Alexa
756 546, and anti-rat Alexa 633. The images of neurons expressing CaMPARI2 were acquired by using a Zeiss LSM
757 700 confocal microscope with a 40x/1.0 Plan-Apochromat oil immersion objective. All parameter settings of the
758 microscope were kept identical across the experimental groups. To enhance green CaMPARI2 fluorescence, a 5%
759 405 nm laser was mixed with a 20% 639 nm laser. To achieve fair comparisons by minimizing the potential biases
760 from day-to-day variations in stimulation, immunostaining, and imaging, similar numbers of animals from each
761 experimental group were tested, immunostained, and imaged side-by-side on the same day.

762 Maximum intensity projections of images were generated from the Z-stacks using Zeiss Zen Lite software.
763 Photoconversion rates of CaMPARI2 were quantified using MATLAB. Cell bodies of neurons expressing

764 CaMPARI2 were automatically segmented using Otsu's thresholding algorithm (87) based on the anti-HA signal
765 intensity on the blue channel, and each image was cropped around the cell bodies with a margin of 50 pixels to the
766 top, bottom, left, and right. Average intensities of green (green CaMPARI2) and red (anti-CaMPARI red) signals
767 were calculated for cell bodies and the background (cropped image area excluding cell bodies), and the Red/Green
768 ratio was calculated as follows: Red/Green ratio = (Average red signal intensity of cell bodies – Average red signal
769 intensity of the background) / (Average green signal intensity of cell bodies – Average green signal intensity of the
770 background). In the analysis of Goro neurons, images in which both sides of the cell bodies were segmented by
771 Otsu's method were included for the subsequent analyses.

772 **Data collection and statistical analyses**

773 Mann–Whitney's U-test was used for pair-wise comparisons and Steel's test (the non-parametric equivalent of
774 Dunnet's test) or Steel–Dwass test (the non-parametric equivalent of Tukey-Kramer test) were used for multiple
775 comparisons. Statistical analyses were performed in KyPlot 5.0 and GraphPad Prism 9. The numbers of samples
776 (n) for all experiments indicate the numbers of biological replicates. Each experiment was repeated at least twice
777 on different days to check the reproducibility, and all data were pooled for statistical analyses unless otherwise
778 noted.

779 **References**

780 1. Dubin AE, Patapoutian A. Nociceptors: the sensors of the pain pathway. J Clin Invest. 2010;120(11):3760-

781 72.

782 2. Burrell BD. Comparative biology of pain: What invertebrates can tell us about how nociception works. J

783 Neurophysiol. 2017;117(4):1461-73.

784 3. Walters ET. Nociceptive Biology of Molluscs and Arthropods: Evolutionary Clues About Functions and

785 Mechanisms Potentially Related to Pain. Front Physiol. 2018;9:1049.

786 4. Reynolds DV. Surgery in the rat during electrical analgesia induced by focal brain stimulation. Science.

787 1969;164(3878):444-5.

788 5. Chen Q, Heinricher MM. Descending Control Mechanisms and Chronic Pain. Current rheumatology

789 reports. 2019;21(5):13.

790 6. Ossipov MH, Morimura K, Porreca F. Descending pain modulation and chronification of pain. Curr Opin

791 Support Palliat Care. 2014;8(2):143-51.

792 7. Arenas OM, Zaharieva EE, Para A, Vasquez-Doorman C, Petersen CP, Gallio M. Activation of planarian

793 TRPA1 by reactive oxygen species reveals a conserved mechanism for animal nociception. Nat Neurosci.

794 2017;20(12):1686-93.

795 8. Sneddon LU. Comparative Physiology of Nociception and Pain. Physiology (Bethesda). 2018;33(1):63-

796 73.

797 9. Ossipov MH, Dussor GO, Porreca F. Central modulation of pain. J Clin Invest. 2010;120(11):3779-87.

798 10. Heinricher MM, Neubert MJ. Neural basis for the hyperalgesic action of cholecystokinin in the rostral
799 ventromedial medulla. J Neurophysiol. 2004;92(4):1982-9.

800 11. Heinricher MM, McGaraughty S, Tortorici V. Circuitry underlying antiopioid actions of cholecystokinin
801 within the rostral ventromedial medulla. J Neurophysiol. 2001;85(1):280-6.

802 12. Marshall TM, Herman DS, Largent-Milnes TM, Badghisi H, Zuber K, Holt SC, et al. Activation of
803 descending pain-facilitatory pathways from the rostral ventromedial medulla by cholecystokinin elicits release of
804 prostaglandin-E(2) in the spinal cord. Pain. 2012;153(1):86-94.

805 13. Xie JY, Herman DS, Stiller CO, Gardell LR, Ossipov MH, Lai J, et al. Cholecystokinin in the rostral
806 ventromedial medulla mediates opioid-induced hyperalgesia and antinociceptive tolerance. J Neurosci.
807 2005;25(2):409-16.

808 14. Roca-Lapirot O, Fossat P, Ma S, Egron K, Trigilio G, Lopez-Gonzalez MJ, et al. Acquisition of analgesic
809 properties by the cholecystokinin (CCK)/CCK2 receptor system within the amygdala in a persistent inflammatory
810 pain condition. Pain. 2019;160(2):345-57.

811 15. Manai M, van Middendorp H, Veldhuijzen DS, Huizinga TWJ, Evers AWM. How to prevent, minimize,
812 or extinguish nocebo effects in pain: a narrative review on mechanisms, predictors, and interventions. Pain reports.
813 2019;4(3):e699.

814 16. Elphick MR, Mirabeau O, Larhammar D. Evolution of neuropeptide signalling systems. J Exp Biol.

815 2018;221(Pt 3).

816 17. Mirabeau O, Joly JS. Molecular evolution of peptidergic signaling systems in bilaterians. Proc Natl Acad

817 Sci U S A. 2013;110(22):E2028-37.

818 18. Jekely G. Global view of the evolution and diversity of metazoan neuropeptide signaling. Proc Natl Acad

819 Sci U S A. 2013;110(21):8702-7.

820 19. Nassel DR, Williams MJ. Cholecystokinin-Like Peptide (DSK) in Drosophila, Not Only for Satiety

821 Signaling. Front Endocrinol (Lausanne). 2014;5:219.

822 20. Tinoco AB, Barreiro-Iglesias A, Yanez Guerra LA, Delroisse J, Zhang Y, Gunner EF, et al. Ancient role

823 of sulfakinin/cholecystokinin-type signalling in inhibitory regulation of feeding processes revealed in an

824 echinoderm. eLife. 2021;10.

825 21. Wu S, Guo C, Zhao H, Sun M, Chen J, Han C, et al. Drosulfakinin signaling in fruitless circuitry

826 antagonizes P1 neurons to regulate sexual arousal in Drosophila. Nat Commun. 2019;10(1):4770.

827 22. Wu F, Deng B, Xiao N, Wang T, Li Y, Wang R, et al. A neuropeptide regulates fighting behavior in

828 Drosophila melanogaster. eLife. 2020;9.

829 23. Mohammad F, Aryal S, Ho J, Stewart JC, Norman NA, Tan TL, et al. Ancient Anxiety Pathways Influence

830 Drosophila Defense Behaviors. Curr Biol. 2016;26(7):981-6.

831 24. Tracey WD, Jr., Wilson RI, Laurent G, Benzer S. painless, a Drosophila gene essential for nociception.

832 Cell. 2003;113(2):261-73.

833 25. Hwang RY, Zhong L, Xu Y, Johnson T, Zhang F, Deisseroth K, et al. Nociceptive neurons protect
834 Drosophila larvae from parasitoid wasps. Curr Biol. 2007;17(24):2105-16.
835 26. Zhong L, Bellemer A, Yan H, Honjo K, Robertson J, Hwang RY, et al. Thermosensory and non-
836 thermosensory isoforms of Drosophila melanogaster TRPA1 reveal heat sensor domains of a thermoTRP channel.
837 Cell Rep. 2012;1(1):43-55.
838 27. Kim SE, Coste B, Chadha A, Cook B, Patapoutian A. The role of Drosophila Piezo in mechanical
839 nociception. Nature. 2012;483(7388):209-12.
840 28. Zhong L, Hwang RY, Tracey WD. Pickpocket is a DEG/ENaC protein required for mechanical nociception
841 in Drosophila larvae. Curr Biol. 2010;20(5):429-34.
842 29. Mauthner SE, Hwang RY, Lewis AH, Xiao Q, Tsubouchi A, Wang Y, et al. Balboa binds to pickpocket in
843 vivo and is required for mechanical nociception in Drosophila larvae. Curr Biol. 2014;24(24):2920-5.
844 30. Babcock DT, Shi S, Jo J, Shaw M, Gutstein HB, Galko MJ. Hedgehog signaling regulates nociceptive
845 sensitization. Curr Biol. 2011;21(18):1525-33.
846 31. Honjo K, Mauthner SE, Wang Y, Skene JH, Tracey WD, Jr. Nociceptor-Enriched Genes Required for
847 Normal Thermal Nociception. Cell Rep. 2016;16(2):295-303.
848 32. Honjo K, Tracey WD, Jr. BMP signaling downstream of the Highwire E3 ligase sensitizes nociceptors.
849 PLoS Genet. 2018;14(7):e1007464.
850 33. Neely GG, Hess A, Costigan M, Keene AC, Goulas S, Langeslag M, et al. A genome-wide Drosophila

851 screen for heat nociception identifies alpha2delta3 as an evolutionarily conserved pain gene. Cell. 2010;143(4):628-
852 38.
853 34. Follansbee TL, Gjelsvik KJ, Brann CL, McParland AL, Longhurst CA, Galko MJ, et al. Drosophila
854 Nociceptive Sensitization Requires BMP Signaling via the Canonical SMAD Pathway. J Neurosci.
855 2017;37(35):8524-33.
856 35. Burgos A, Honjo K, Ohyama T, Qian CS, Shin GJ, Gohl DM, et al. Nociceptive interneurons control
857 modular motor pathways to promote escape behavior in Drosophila. eLife. 2018;7.
858 36. Kaneko T, Macara AM, Li R, Hu Y, Iwasaki K, Dunnings Z, et al. Serotonergic Modulation Enables
859 Pathway-Specific Plasticity in a Developing Sensory Circuit in Drosophila. Neuron. 2017;95(3):623-38 e4.
860 37. Takagi S, Cocanougher BT, Niki S, Miyamoto D, Kohsaka H, Kazama H, et al. Divergent Connectivity
861 of Homologous Command-like Neurons Mediates Segment-Specific Touch Responses in Drosophila. Neuron.
862 2017;96(6):1373-87 e6.
863 38. Dason JS, Cheung A, Anreiter I, Montemurri VA, Allen AM, Sokolowski MB. Drosophila melanogaster
864 foraging regulates a nociceptive-like escape behavior through a developmentally plastic sensory circuit. Proc Natl
865 Acad Sci U S A. 2020;117(38):23286-91.
866 39. Hu Y, Wang C, Yang L, Pan G, Liu H, Yu G, et al. A Neural Basis for Categorizing Sensory Stimuli to
867 Enhance Decision Accuracy. Curr Biol. 2020;30(24):4896-909 e6.
868 40. Chin MR, Tracey WD, Jr. Nociceptive Circuits: Can't Escape Detection. Curr Biol. 2017;27(16):R796-R8.

869 41. Hu C, Petersen M, Hoyer N, Spitzweck B, Tenedini F, Wang D, et al. Sensory integration and
870 neuromodulatory feedback facilitate Drosophila mechanonociceptive behavior. Nat Neurosci. 2017;20(8):1085-95.
871 42. Im SH, Takle K, Jo J, Babcock DT, Ma Z, Xiang Y, et al. Tachykinin acts upstream of autocrine Hedgehog
872 signaling during nociceptive sensitization in Drosophila. eLife. 2015;4:e10735.
873 43. Bachtel ND, Hovsepian GA, Nixon DF, Eleftherianos I. Allatostatin C modulates nociception and
874 immunity in Drosophila. Scientific reports. 2018;8(1):7501.
875 44. Aldrich BT, Kasuya J, Faron M, Ishimoto H, Kitamoto T. The amnesiac gene is involved in the regulation
876 of thermal nociception in Drosophila melanogaster. J Neurogenet. 2010;24(1):33-41.
877 45. Chen X, Peterson J, Nachman RJ, Ganetzky B. Drosulfakinin activates CCKLR-17D1 and promotes larval
878 locomotion and escape response in Drosophila. Fly (Austin). 2012;6(4):290-7.
879 46. Kubiak TM, Larsen MJ, Burton KJ, Bannow CA, Martin RA, Zantello MR, et al. Cloning and functional
880 expression of the first Drosophila melanogaster sulfakinin receptor DSK-R1. Biochem Biophys Res Commun.
881 2002;291(2):313-20.
882 47. Nichols R, Lim IA. Spatial and temporal immunocytochemical analysis of drosulfakinin (Dsk) gene
883 products in the Drosophila melanogaster central nervous system. Cell Tissue Res. 1996;283(1):107-16.
884 48. Veenstra JA, Agricola HJ, Sellami A. Regulatory peptides in fruit fly midgut. Cell Tissue Res.
885 2008;334(3):499-516.
886 49. Soderberg JA, Carlsson MA, Nassel DR. Insulin-Producing Cells in the Drosophila Brain also Express

887 Satiety-Inducing Cholecystokinin-Like Peptide, Drosulfakinin. Front Endocrinol (Lausanne). 2012;3:109.

888 50. Park D, Veenstra JA, Park JH, Taghert PH. Mapping peptidergic cells in Drosophila: where DIMM fits in.

889 PLoS One. 2008;3(3):e1896.

890 51. Nassel DR, Winther AM. Drosophila neuropeptides in regulation of physiology and behavior. Prog

891 Neurobiol. 2010;92(1):42-104.

892 52. Deng B, Li Q, Liu X, Cao Y, Li B, Qian Y, et al. Chemoconnectomics: Mapping Chemical Transmission

893 in Drosophila. Neuron. 2019;101(5):876-93 e4.

894 53. Ohyama T, Schneider-Mizell CM, Fetter RD, Aleman JV, Franconville R, Rivera-Alba M, et al. A

895 multilevel multimodal circuit enhances action selection in Drosophila. Nature. 2015;520(7549):633-9.

896 54. Luo J, Shen WL, Montell C. TRPA1 mediates sensation of the rate of temperature change in Drosophila

897 larvae. Nat Neurosci. 2017;20(1):34-41.

898 55. Nicolai LJ, Ramaekers A, Raemaekers T, Drozdzecki A, Mauss AS, Yan J, et al. Genetically encoded

899 dendritic marker sheds light on neuronal connectivity in Drosophila. Proc Natl Acad Sci U S A.

900 2010;107(47):20553-8.

901 56. Fosque BF, Sun Y, Dana H, Yang CT, Ohyama T, Tadross MR, et al. Neural circuits. Labeling of active

902 neural circuits in vivo with designed calcium integrators. Science. 2015;347(6223):755-60.

903 57. Moeyaert B, Holt G, Madangopal R, Perez-Alvarez A, Fearey BC, Trojanowski NF, et al. Improved

904 methods for marking active neuron populations. Nat Commun. 2018;9(1):4440.

905 58. Feinberg EH, Vanhoven MK, Bendesky A, Wang G, Fetter RD, Shen K, et al. GFP Reconstitution Across
906 Synaptic Partners (GRASP) defines cell contacts and synapses in living nervous systems. Neuron. 2008;57(3):353-
907 63.
908 59. Gordon MD, Scott K. Motor control in a Drosophila taste circuit. Neuron. 2009;61(3):373-84.
909 60. Roy S, Huang H, Liu S, Kornberg TB. Cytoneme-mediated contact-dependent transport of the Drosophila
910 decapentaplegic signaling protein. Science. 2014;343(6173):1244624.
911 61. Gonzalez-Mendez L, Seijo-Barandiaran I, Guerrero I. Cytoneme-mediated cell-cell contacts for Hedgehog
912 reception. eLife. 2017;6.
913 62. Macpherson LJ, Zaharieva EE, Kearney PJ, Alpert MH, Lin TY, Turan Z, et al. Dynamic labelling of
914 neural connections in multiple colours by trans-synaptic fluorescence complementation. Nat Commun.
915 2015;6:10024.
916 63. Talay M, Richman EB, Snell NJ, Hartmann GG, Fisher JD, Sorkac A, et al. Transsynaptic Mapping of
917 Second-Order Taste Neurons in Flies by trans-Tango. Neuron. 2017;96(4):783-95 e4.
918 64. Hamada FN, Rosenzweig M, Kang K, Pulver SR, Ghezzi A, Jegla TJ, et al. An internal thermal sensor
919 controlling temperature preference in Drosophila. Nature. 2008;454(7201):217-20.
920 65. Zhong L, Bellemer A, Yan H, Ken H, Jessica R, Hwang RY, et al. Thermosensory and nonthermosensory
921 isoforms of Drosophila melanogaster TRPA1 reveal heat-sensor domains of a thermoTRP Channel. Cell Rep.
922 2012;1(1):43-55.

923 66. Chen X, Ganetzky B. A neuropeptide signaling pathway regulates synaptic growth in Drosophila. J Cell
924 Biol. 2012;196(4):529-43.
925 67. Im SH, Patel AA, Cox DN, Galko MJ. Drosophila Insulin receptor regulates the persistence of injury-
926 induced nociceptive sensitization. Dis Model Mech. 2018;11(5).
927 68. van den Pol AN. Neuropeptide transmission in brain circuits. Neuron. 2012;76(1):98-115.
928 69. Pommier B, Beslot F, Simon A, Pophillat M, Matsui T, Dauge V, et al. Deletion of CCK2 receptor in mice
929 results in an upregulation of the endogenous opioid system. J Neurosci. 2002;22(5):2005-11.
930 70. Noble F, Roques BP. Phenotypes of mice with invalidation of cholecystokinin (CCK(1) or CCK(2))
931 receptors. Neuropeptides. 2002;36(2-3):157-70.
932 71. Baber NS, Dourish CT, Hill DR. The role of CCK caerulein, and CCK antagonists in nociception. Pain.
933 1989;39(3):307-28.
934 72. Suh HH, Tseng LF. Differential effects of sulfated cholecystokinin octapeptide and proglumide injected
935 intrathecally on antinociception induced by beta-endorphin and morphine administered intracerebroventricularly in
936 mice. Eur J Pharmacol. 1990;179(3):329-38.
937 73. Liu Y, Latremoliere A, Li X, Zhang Z, Chen M, Wang X, et al. Touch and tactile neuropathic pain
938 sensitivity are set by corticospinal projections. Nature. 2018;561(7724):547-50.
939 74. Curtright A, Rosser M, Goh S, Keown B, Wagner E, Sharifi J, et al. Modeling Nociception in Zebrafish:
940 A Way Forward for Unbiased Analgesic Discovery. Plos One. 2015;10(1).

941 75. Milinkeviciute G, Gentile C, Neely GG. Drosophila as a tool for studying the conserved genetics of pain.
942 Clinical genetics. 2012;82(4):359-66.
943 76. Tobin DM, Bargmann CI. Invertebrate nociception: Behaviors, neurons and molecules. Journal of
944 Neurobiology. 2004;61(1):161-74.
945 77. Malafoglia V, Bryant B, Raffaeli W, Giordano A, Bellipanni G. The zebrafish as a model for nociception
946 studies. Journal of Cellular Physiology. 2013;228(10):1956-66.
947 78. Khuong TM, Wang QP, Manion J, Oyston LJ, Lau MT, Towler H, et al. Nerve injury drives a heightened
948 state of vigilance and neuropathic sensitization in Drosophila. Science advances. 2019;5(7):eaaw4099.
949 79. Kondo S, Takahashi T, Yamagata N, Imanishi Y, Katow H, Hiramatsu S, et al. Neurochemical
950 Organization of the Drosophila Brain Visualized by Endogenously Tagged Neurotransmitter Receptors. Cell Rep.
951 2020;30(1):284-97 e5.
952 80. Wong AM, Wang JW, Axel R. Spatial representation of the glomerular map in the Drosophila
953 protocerebrum. Cell. 2002;109(2):229-41.
954 81. Ren Q, Awasaki T, Huang YF, Liu Z, Lee T. Cell Class-Lineage Analysis Reveals Sexually Dimorphic
955 Lineage Compositions in the Drosophila Brain. Curr Biol. 2016;26(19):2583-93.
956 82. Kondo S, Ueda R. Highly improved gene targeting by germline-specific Cas9 expression in Drosophila.
957 Genetics. 2013;195(3):715-21.
958 83. Bischof J, Bjorklund M, Furger E, Schertel C, Taipale J, Basler K. A versatile platform for creating a

959 comprehensive UAS-ORFeome library in Drosophila. Development. 2013;140(11):2434-42.

960 84. Marder E, Calabrese RL, Nusbaum MP, Trimmer B. Distribution and partial characterization of

961 FMRFamide-like peptides in the stomatogastric nervous systems of the rock crab, Cancer borealis, and the spiny

962 lobster, Panulirus interruptus. J Comp Neurol. 1987;259(1):150-63.

963 85. Chen TW, Wardill TJ, Sun Y, Pulver SR, Renninger SL, Baohan A, et al. Ultrasensitive fluorescent

964 proteins for imaging neuronal activity. Nature. 2013;499(7458):295-300.

965 86. Feng Y, Ueda A, Wu CF. A modified minimal hemolymph-like solution, HL3.1, for physiological

966 recordings at the neuromuscular junctions of normal and mutant Drosophila larvae. J Neurogenet. 2004;18(2):377-

967 402.

968 87. Otsu N. Threshold Selection Method from Gray-Level Histograms. Ieee T Syst Man Cyb. 1979;9(1):62-

969 6.